Model atomic systems in intense laser fields: exact time-dependent density functional and Floquet theory

Dissertation
zur
Erlangung des akademischen Grades
doctor rerum naturalium (Dr. rer. nat.)
der Mathematisch-Naturwissenschaftlichen Fakultät
der Universität Rostock

vorgelegt von

Varun Kapoor, geb. am September 28, 1983 in Srinagar

aus Indien

Datum der Einreichung: September 25, 2013

urn:nbn:de:gbv:28-diss2014-0048-4

BETREUER:
Prof. Dr. Dieter Bauer
(Institut für Physik, Universität Rostock)

GUTACHTER:
Prof. Dr. Dieter Bauer
(Institut für Physik, Universität Rostock)
Prof. Dr. Thomas Fennel
(Institut für Physik, Universität Rostock)

Datum der Verteidigung: December 18, 2013

ABSTRACT

Describing the quantum dynamics in strong time-dependent external fields is challenging for at least two reasons. Firstly, the external driver has to be treated in a non-perturbative way. Secondly, correlations, responsible for phenomena such as single-photon double ionization, non-sequential double ionization, autoionization, Auger decay etc., have to be taken into account.

The *ab initio* solution of the time-dependent Schrödinger equation for a many-body system is feasible for only a few constituents. Density functional theory (DFT) has been successful in overcoming the exponentially increasing complexity of solving the stationary Schrödinger equation in electronic structure applications. Its time-dependent extension (TDDFT) is widely applied within the linear response domain. However, its success when it comes to highly correlated electron dynamics in, for instance, strong laser fields, is very limited, reasons being the lack of a sufficiently accurate exchange-correlation potential in the Kohn-Sham equation and functionals for the relevant observables. Numerically exactly solvable model systems are hence very useful to proceed with the further development of TDDFT. In this thesis, the exact exchange-correlation potential for the highly correlated process of autoionization in a model Helium atom is constructed.

Besides applying a suitable many-body technique one may try to employ the time-periodicity of external drivers such as laser fields. The Floquet theorem allows to rewrite partial differential equations with time-periodic coefficients as sets of time-independent algebraic equations. If the Floquet theorem could also be applied to the time-dependent Kohn-Sham equation of TDDFT the time-dependent many-body problem could be reduced to a time-independent one. In this thesis, it is investigated under which circumstances this is possible. To that end a method is introduced to extract the information about light-induced states (Floquet states) and their populations directly from the real-time many-body wavefunction also in cases where the Hamiltonian is not strictly time-periodic, i.e., in a time-resolved way.

ZUSAMMENFASSUNG

Die Beschreibung von Quantendynamik in starken, zeitabhängigen, externen Feldern stellt aus mindestens zwei Gründen eine Herausforderung dar. Erstens muss der externe Treiber nicht-störungstheoretisch behandelt werden. Zweitens müssen Korrelationen berücksichtigt werden, die beispielsweise für Phänomene wie Einzelphoton-Doppelionisation, nichtsequentielle Ionisation, Autoionisation und Auger-Zerfall etc. verantwortlich sind.

Die ab-initio Lösung der zeitabhängigen Schrödinger-Gleichung für ein Vielteilchensystem ist nur für einige wenige Konstituenten möglich. Dichtefunktionaltheorie (DFT) war sehr erfolgreich darin, die exponentiell anwachsende Komplexität der Lösung der stationären Schrödinger-Gleichung in elektronischen Strukturrechnungen zu überwinden. Ihre zeitabhängige Erweiterung (TDDFT) wird verbreitet im Bereich der linearen Antworttheorie angewandt. Leider ist der Erfolg im Fall hoch-korrelierter Elektronendynamik in, z.B., starken Laserfeldern sehr beschränkt. Gründe dafür sind das Fehlen eines hinreichend genauen Austausch-Korrelationspotentials in der Kohn-Sham-Gleichung und Funktionale für die relevanten Observable. Numerisch exakt lösbare Modellsysteme sind daher sehr nützlich, um mit der Weiterentwicklung von TDDFT voranzuschreiten. In dieser Arbeit wird das exakte Austausch-Korrelationspotential für den hoch-korrelierten Prozess der Autoionisation in einem Modellhelium-Atom konstruiert.

Neben der Anwendung einer angemessenen Vielteilchenmethode könnte man versuchen, die Zeitperiodizität externer Treiber wie z.B. Laserfelder auszunutzen. Das Floquet-Theorem erlaubt es, partielle Differentialgleichungen mit zeitperiodischen Koeffizienten als Satz zeitunabhängiger, algebraischer Gleichungen umzuschreiben. Falls das Floquet-Theorem auch auf die zeitabhängige Kohn-Sham-Gleichung der TDDFT anwendbar wäre, könnte das zeitabhängige Vielteilchenproblem auf ein zeitunabhängiges reduziert werden. In dieser Arbeit wird untersucht, unter welchen Umständen dies möglich ist. Zu diesem Zweck wird eine Methode eingeführt, mit der Informationen über lichtinduzierte Zustände (Floquet-Zustände) und deren Besetzungen direkt

aus der zeitabhängigen Vielteilchenwellenfunktion extrahiert werden können, auch in den Fällen, wo der Hamilton-Operator nicht streng zeitperiodisch ist, also in einer zeitaufgelösten Art und Weise.

The following peer-reviewed articles were published in connection with this thesis:

- *Floquet analysis of real-time wavefunctions without solving the Floquet equation,*

  V. Kapoor, D. Bauer, Phys. Rev. A **85**, 023407 (2012)

- *Periodicity of the time-dependent Kohn-Sham equation and the Floquet theorem,*

  V. Kapoor, M. Ruggenthaler, D. Bauer, Phys. Rev. A **87**, 042521 (2013)

The following article is in preperation for publication in a peer-reviewed journal.

- *Exact exchange correlation potentials for autoionization in TDDFT,*

  V. Kapoor, D. Bauer

The following talks were presented in connection with this thesis work (speaker underlined) .

- *Exact exchange-correlation potentials for worst case time-dependent density functional theory scenarios ,*

  V. Kapoor, D. Bauer.

  Research Seminar, 4 June 2013, Rostock, Germany.

- *Autoionization in time dependent density functional theory,*

  V. Kapoor, D. Bauer.

  Spring meeting of German Physical Society, 17-23 March 2013, Hannover, Germany.

- *Correlated laser-driven electron dynamics in time-dependent density functional theory and beyond,*

  D. Bauer, V. Kapoor.

  LPHYS 2012, Calgary, Canada, July 23-27, 2012.

- *Decay of hollow states in time dependent density functional theory,*

  V. Kapoor, D. Bauer.

  Spring meeting of German Physical Society, 12-16 March 2012, Stuttgart, Germany.

- *Applicability of the Floquet theorem to time dependent density functionla theory,*

  V. Kapoor, D. Bauer.

  Spring meeting of German Physical Society, 13-18 March 2011, Dresden, Germany.

- *Floquet analysis of real-time wavefunctions without solving the Floquet equation,*

  V. Kapoor, D. Bauer.

  Max Planck Institute for Nuclear Physics. February 2010, Heidelberg, Germany,

ACKNOWLEDGEMENTS

First of all I would like to extend my gratitude to my supervisor Prof. Dr. Dieter Bauer. He not only gave me an opportunity to work in his research group but also provided a very conductive atmosphere to perform my research work. Without his constant support, advice and constructive criticism this thesis would not have seen the light of the day. I would also like to thank the colleagues at the Max Planck Institute for Nuclear Physics, Heidelberg for their friendliness shown when I started working in Dieter's group. My thanks also extend to our group secretary, Frau Hertzfeldt for aiding in the administrative tasks all along. Dr. Tatyana Liseykina made a wonderful officemate and was always willing to lend a helping hand when needed. It was also fun to work with Julius Rapp as a collaborator during the beginning of his master's work. Our previous group member Dr. M. Ruggenthaler deserves special thanks for the fruitful collaboration which lead to an interesting publication.

My wife Samta deserves appreciation for her understanding and support provided during my life as a doctoral student. I would also like to acknowledge my family and friends for being understanding all throught.

CONTENTS

1

INTRODUCTION

The dynamics of non-relativistic microscopic particles are governed by the time-dependent Schrödinger equation (TDSE). The analytical solution of the TDSE for a many-body, N-particle system is in general unknown. Numerically, the TDSE can be solved for a many-body system with only very few constituents ($N \leq 2$). The numerical solution of the TDSE may be attained by reducing the dimensionality of the system under consideration because for atomic systems exposed to laser pulses the quantum dynamics proceeds predominantly along the laser polarization direction. With such a restriction the TDSE can be solved exactly for up to three-electron models.

Although the time-dependent many-body wave function contains all the system information, extracting insight into the dynamics of the system from it may not always be straightforward. One such example is the determination of the populated light-induced states when an atomic system is exposed to a laser pulse. For a time-periodic Hamiltonian the time-dependent Schrödinger wave function can be expanded in a time-independent basis known as the light-induced or Floquet states [1–4]. The conventional Floquet approaches assume that the laser is always on and hence lack the information about the Floquet states populated during the laser-atom interaction. The population of the Floquet states depends on the specific laser parameters including the laser intensity, frequency and pulse shape. Moreover, for laser pulses the Hamiltonian is not strictly periodic. In Chapter 4 a technique is developed specifically to extract the information about the laser-dressed states and their populations from the time-dependent Schrödinger wave function.

To go beyond the restriction of $N = 3$ electron systems which can be solved via the full many-body TDSE, approximate wave function based methods were proposed such as the time-dependent Hartree-Fock (TDHF) or the configuration interaction (CI) methods. The HF method ignores many-body correlation effects. The CI does take into account the correlation effects but if fully included to obtain the many-body

wave function, the method becomes as expensive as solving the TDSE. It has been proven that the ground state of a many electron system is uniquely described by the single particle density (Hohenberg-Kohn (HK) theorem) [5, 6]. The single particle density is a three dimensional spatial object, in contrast to the many-body wave function depending on $3N$ spatial coordinates. For the time-independent case the single particle density gives the ground state properties of the system and is widely used to obtain structural properties of a many-body N-particle system, where N can be quite large. Ground state DFT has been extended to the time-dependent case, leading to time-dependent density functional theory (TDDFT) [7]. In practise, the interacting system is replaced by an auxiliary non-interacting system for which the Kohn-Sham (KS) equation is solved [8–12]. In the latter, an exchange-correlation potential needs to be approximated, as the exact one is unknown. Moreover, some of the relevant observables are not known as functionals of the single particle density and therefore need to be approximated as well [13]. Due to lack of the true many-body correlations the ground state properties deviate from the true values while the time-dependent dynamics can be completely different from the true dynamics of the system under consideration. In this work numerically exactly solvable model systems are considered so that the exact exchange-correlation potential of TDDFT can be constructed. In that way better approximations to the exchange-correlation potential that include essential physical effects may be developed. With currently available approximations highly correlated processes like single photon double ionization, autoionization, charge-transfer and resonant interactions (Rabi floppings, [14, 15]) are not properly incorporated. In Chapter 6 an exact-exchange correlation potential is constructed for a one-dimensional model Helium atom when autoionization occurs via the resonant excitation of multiply excited states.

If Floquet theory can be combined with TDDFT, time-independent equations for many-body systems in time-periodic external potentials could be derived, thus avoiding the solution of the time-dependent KS equation. However, in Chapter 5 it will be shown that the KS Hamiltonian is not strictly time-periodic so that the Floquet theorem is not applicable in this case. In Chapter 2 the basic processes occurring in intense laser atom interactions are introduced while in Chapter 3 the essential theoretical tools required to simulate such processes are covered.

Details about the computational aspects are briefly included in the appendices.

In this work atomic units ($|e| = m_e = \hbar = 4\pi\epsilon_0 = 1$) are used unless stated otherwise.

2

INTENSE LASER-MATTER INTERACTION

2.1 PROCESSES IN INTENSE LASER-ATOM INTERACTION

Atomic and molecular systems exposed to coherent light sources provide not only deep insight into the quantum nature of microscopic particles but also enables one to capture the *fast* dynamics of the electronic processes. Electronic processes happen at attosecond timescale ($\sim 10^{-18}$ sec). In order to be able to "photograph" the motion of the microscopic particles the coherent light sources must have a coherence time of at least a few attoseconds. Much advancement in laser technology is aimed at producing short and intense laser pulses with such coherence times. Novel theoretical tools going beyond conventional perturbation theory have been developed as the electric fields associated with nowadays available laser intensities easily compete or even exceed binding forces in atoms and molecules. The theoretical and experimental studies in laser-matter interaction have been productive in predicting, observing and explaining novel phenomena not accessible to low field spectroscopic methods.

In the following we introduce the basic phenomena occurring in intense laser-atom interaction.

2.1.1 *Above-threshold ionization of atoms and harmonic generation*

In intense laser fields electrons can absorb more photons than needed to reach the continuum, leading to higher photo-electron energies than expected in the lowest-order photo effect [16, 17]. If an electron absorbs only the minimum number of photons n required to reach the continuum its kinetic-energy is given by

$$\mathcal{E} = n\omega_1 - I_p, \tag{1}$$

where I_p is the ionization potential of the atom and ω_1 is the laser frequency. If the electron absorbs m more photons, the energy is

$$\mathcal{E} = (n+m)\omega_1 - I_p. \tag{2}$$

One also has to consider the *quiver* motion of the electron in the oscillatory field of the laser once it is in the continuum. Due to this quiver motion the effective ionization potential of the atom is increased. The quiver energy of the electron for a linearly polarized laser pulse with intensity I and frequency ω_1 is given by

$$U_p = \frac{I}{4\omega_1^2} \tag{3}$$

so that

$$\mathcal{E} = (n+m)\omega_1 - I_p - U_p. \tag{4}$$

We can see that as the intensity of the laser is increased the energy of the photo-electron reduces to zero for a given $n+m$. This is referred to as the $n+m$ channel closing as $n+m$ photons are no longer sufficient for the electron to reach the continuum but $n+m+1$ are required. The observed photo-electron spectra are known as above-threshold ionization (ATI) spectra. Figure 1 shows experimentally obtained ATI spectrum for the hydrogen atom for two different intensities, as reported in [18]. One can notice many interesting features in the spectra. First, the peaks are separated by $\hbar\omega_1$. The electron yield drops drastically after 14 eV in the plot for the low intensity and 32 eV for the high intensity. There is a plateau between 10-14 eV in the plot for the low intensity and 25-32 eV for the high intensity.

We perform a TDSE simulation to obtain the ATI spectrum. Figure 2 shows the simulation result for the hydrogen atom exposed to a 10-cycle sinusoidal, 800-nm laser pulse with the intensity of 2.3×10^{14}. The peaks are separated by the laser frequency and the cutoff for the plateau is around $10U_p$, although the yield is not constant over the plateau. These are the universal features found in the spectra and a simple explanation for the existence of the plateau and the sharp cutoff can be understood by the following energy considerations. The maximum kinetic drift energy an electron can gain in a femtosecond laser pulse is $2U_p$. The electron can also re-scatter from the parent ion and due to one such rescattering event the electron may have $10U_p$ of kinetic energy after the laser pulse.

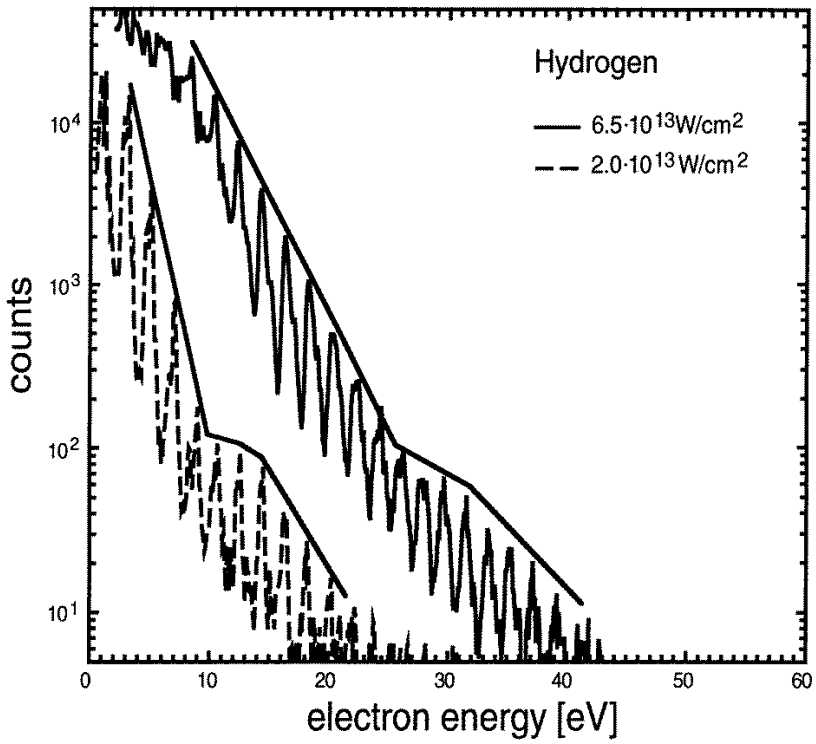

Figure 1: ATI spectrum for the H atom for intensities 2.0×10^{13} and 6.5×10^{13} W/cm^2, $\omega_1 = 0.072$ (630 nm), pulse duration=50 fs [18].

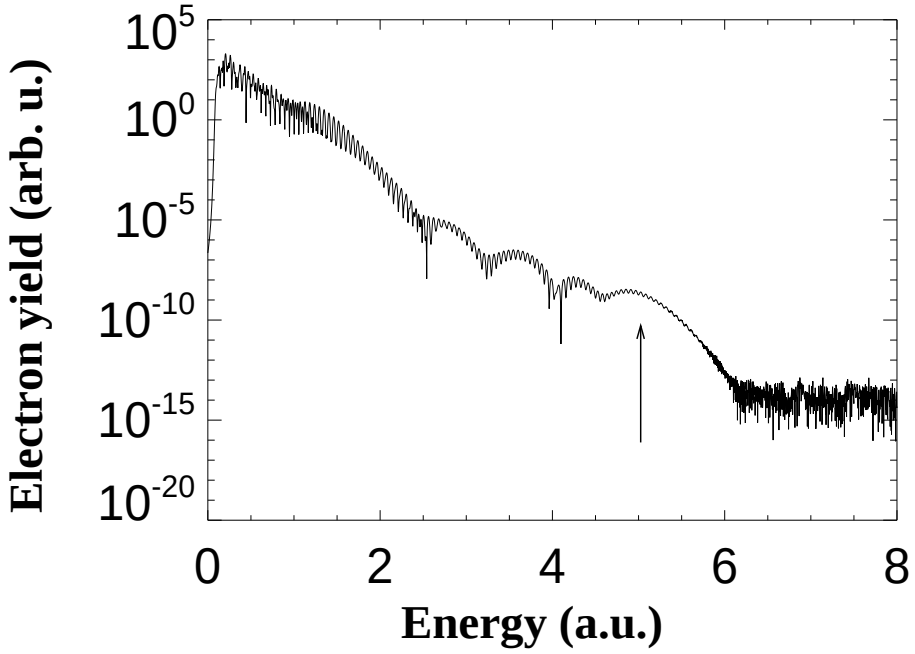

Figure 2: ATI spectrum for H atom for intensity $2.3 \times 10^{14}\ W/\mathrm{cm}^2$, $\omega_1 = 0.056$ (800 nm), 10 cycle sinusoidal pulse. Individual peaks separated by ω_1 are visible. The arrow indicates the classical $10U_p$ cut-off for one rescattering event.

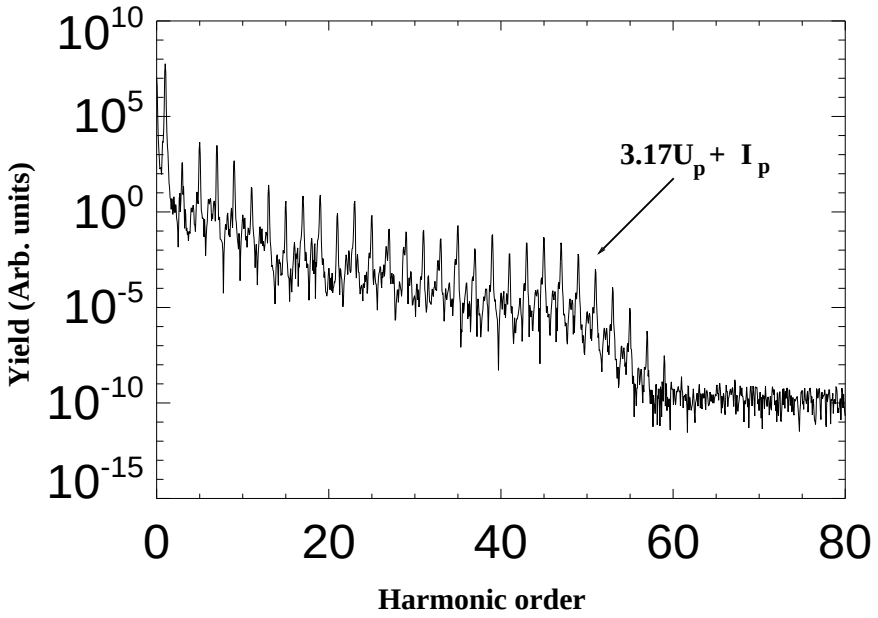

Figure 3: Harmonic spectrum for He^+ atom obtained by Fourier transforming the dipole moment. Laser parameters are specified in the text.

Besides rescattering from the parent ion the electron can also recombine upon releasing the energy by emission of a photon. This process is called (high) harmonic generation. Since the electron reached the continuum by absorbing $n + m$ photons, energy conservation requires that it also emits the same energy, but it can do so by emitting just a single photon, whose frequency is

$$\omega = (n + m)\omega_1. \tag{5}$$

As an example for a high harmonic spectrum we consider a singly ionized Helium atom exposed to 290-nm laser pulse of intensity 5.4×10^{15} W/cm^2 with a 14 cycle trapezoidal laser pulse (2 cycle ramp up and down). To obtain the spectrum of the emitted radiation the dipole moment is Fourier-transformed. The resulting harmonic strength is plotted in Fig. 3 versus the harmonic order. The cutoff lies around the 44th harmonic.

The cutoff in the harmonic order can be explained by the following energy considerations. When the electron returns and recombines with the

parent ion the energy of the emitted photon in terms of energy of the electron is given by

$$\omega = \mathcal{E} + |\mathcal{E}_f|. \tag{6}$$

Here, $\mathcal{E}_f$ refers to the energy of the bound state finally occupied by the electron. In the case the electron recombines with the initial state $|\mathcal{E}_f| = I_p$. The maximum kinetic energy an electron can have when it returns to the ion is $3.17U_p$, hence the cutoff energy in the harmonic spectrum is given by [19]

$$\omega = 3.17U_p + |\mathcal{E}_f|. \tag{7}$$

Due to the high values of electron kinetic energy achieved during the intense laser fields high harmonic orders are obtained. The high harmonics furthermore do not decay exponentially with their harmonic order but exhibit a plateau due to which one can achieve high intensities at short wavelengths. This process is used to produce high-frequency, intense laser sources and has contributed in advancing the laser technology [20].

For the range of laser intensities and frequencies we are interested in certain approximations can be applied while modelling the laser atom interaction. These approximations along with their justification is the subject of discussion of the next section.

2.2 dipole approximation and laser as a classical field

Any electromagnetic field can be described by its vector potential $\mathbf{A}(\mathbf{r}, t)$ which has a spatial ($\mathbf{r}$) and a temporal (t) dependence. The Hamiltonian, $\hat{H}(t)$ for an electron moving in a binding potential $\hat{V}(r)$ and interacting with an electromagnetic field reads

$$\hat{H}(t) = \frac{1}{2}[\mathbf{p} + \mathbf{A}(\mathbf{r}, t)]^2 + \hat{V}(r). \tag{8}$$

The probability of finding the electron at a certain space-time point is given by

$$|\langle \mathbf{r}|\psi(t)\rangle|^2 \tag{9}$$

with $\psi(t)$ governed by the Schrödinger equation

$$\hat{H}(t)|\psi(t)\rangle = i\partial_t|\psi(t)\rangle. \tag{10}$$

If the laser wavelength λ is much larger than the spatial extent of the probability distribution of the electron, one can ignore the spatial dependence in $\mathbf{A}(\mathbf{r}, t)$. The laser field is then completely specified by $\mathbf{A}(t)$. This approximation is reffered to as the dipole approximation [21] which is applicable for a wide range of commonly used wavelengths in experiments and simulations and applied in this thesis.

Another approximation used in theory is to neglect the quantum nature of the radiation field. This implies that the laser field is not quantized and is treated as a classical field. This approximation holds true if the photon density exceeds 1 per cubic wavelength [22] and the electromagnetic field is described by a coherent state. Both is the case for laser fields considered in this thesis.

3

THEORETICAL TOOLS

3.1 TIME-DEPENDENT SCHRÖDINGER EQUATION

The dynamics of non-relativistic charged particles in an electromagnetic field is described exactly via the time-dependent Schrödinger equation (TDSE).

For electronic systems the Hamiltonian can be written as

$$\hat{H}(t) = \hat{T} + \hat{V}_{\text{ee}} + \hat{V}(t) \tag{11}$$

with the kinetic energy operator

$$\hat{T} = \sum_{i=1}^{N} -\frac{\nabla_i^2}{2}, \tag{12}$$

the electron-electron interaction potential

$$\hat{V}_{\text{ee}} = \frac{1}{2} \sum_{i \neq j, i=1}^{N} v_{\text{ee}}(|\mathbf{r}_i - \mathbf{r}_j|), \tag{13}$$

and the external potential

$$\hat{V}(t) = \sum_{i=1}^{N} [v(\mathbf{r}_i) + \mathbf{p}_i \mathbf{A}(t)]. \tag{14}$$

$v(\mathbf{r}_i)$ is the electron-nuclear interaction potential (nucleus is assumed static). The term $\mathbf{p}_i \mathbf{A}(t)$ originates from the square bracket squared in (8).[1] The equation of motion for the many-body N-electron wave function $\psi(\vec{\mathbf{r}}, t)$ exposed to a laser field is given by the time-dependent Schrödinger equation,

[1] The purely time-dependent $\mathbf{A}^2(t)$ also originating from the square bracket squared in (8) can be transformed-away via a contact transformation in dipole approximation.

$$\mathrm{i}\frac{\partial}{\partial t}|\psi(t)\rangle = \hat{H}(t)|\psi(t)\rangle. \tag{15}$$

The Hamiltonian in (14) is written in velocity gauge. In dipole approximation a gauge transformation $U(t) = \exp[\mathrm{i}\mathbf{r}\mathbf{A}(t)]$ transforms $\psi(\mathbf{r}, t)$ to $\psi_2(\mathbf{r}, t)$, and instead of (14)

$$\hat{V}(t) = \sum_{i=1}^{N}[v(\mathbf{r}_i) + \mathbf{r}_i\mathbf{E}(t)] \qquad \text{(length gauge)} \tag{16}$$

arises. Since the observables are the same in all gauges, any gauge can be used for the computation of the wave function. The length gauge has a disadvantage that the laser interaction term $\mathbf{r}\mathbf{E}(t)$ grows with distance $\mathbf{r}$ from the nucleus.

Solving the TDSE (15) is computationally challenging in any gauge as the TDSE-wave function is a $3N$-dimensional object. For increasing N one encounters the so-called exponential wall [8] because the size of the numerical grid to represent the N-body wave function scales exponentially with N. Our goal is to obtain the exact solution of the TDSE when the electromagnetic field is a strong laser field. As pointed out before, the dynamics in this case occur predominantly along the laser polarization direction. For that reason models in which 1–3 [23] electrons are restricted to move in polarization direction only have been introduced in the early 90's [24] and extensively used ever since [25–29] .

3.1.1 *Low-dimensional model systems*

For a two-electron system with a fixed nucleus the effective Hamiltonian in the length gauge (16) reads

$$\begin{aligned}\hat{H}(t) &= -\frac{1}{2}\frac{\partial^2}{\partial x^2} - \frac{1}{2}\frac{\partial^2}{\partial y^2} + V(x,y) + (x+y)E(t) \\ &= \hat{H}_0 + \hat{W}(x,y,t), \qquad \hat{W}(x,y,t) = (x+y)E(t),\end{aligned} \tag{17}$$

with

$$\hat{H}_0 = -\frac{1}{2}\frac{\partial^2}{\partial x^2} - \frac{1}{2}\frac{\partial^2}{\partial y^2} + V(x,y), \qquad E(t) = \hat{E}\cos\omega t. \tag{18}$$

Here, x and y are the coordinates of the "first" and the "second" electron. The potential $V(x,y)$ reads

$$V(x,y) = -\frac{Z}{\sqrt{x^2+\epsilon}} - \frac{Z}{\sqrt{y^2+\epsilon}} + \frac{1}{\sqrt{(x-y)^2+\epsilon}}, \tag{19}$$

where the first two terms describe the interaction with the nucleus and the third the electron-electron repulsion. Z is the nuclear charge. In one-dimension, the softening parameter ϵ is added to ensure that the two electrons can pass by each other and the nucleus without encountering the Coulomb singularity at the origin ($x = 0, y = 0$). The softening parameter can be chosen such that, e.g., the ground state energy of the "real" atom is matched [26, 28–31].

The initial state required as a starting point for a time-dependent problem is usually an eigenstate of the stationary Schrödinger equation

$$\hat{H}_0|\Psi_0\rangle = \mathcal{E}_0|\Psi_0\rangle. \tag{20}$$

The above equation gives the ground state wave function and its energy.

Projecting the space-spin states onto the wave function gives its representation in the space-spin basis

$$\langle x\sigma_1, y\sigma_2|\Psi(t)\rangle = \Psi(x\sigma_1, y\sigma_2, t). \tag{21}$$

Here, σ_1 is the spin variable for the first electron and σ_2 is for the second. In two dimensions the space and spin variables factorize, hence a spin-singlet state for example can be written as

$$\Psi(x\sigma_1, y\sigma_2, t) = \Psi(x, y, t)\frac{1}{\sqrt{2}}\left(|\uparrow_1\rangle|\downarrow_2\rangle - |\downarrow_1\rangle|\uparrow_2\rangle\right). \tag{22}$$

The Hamiltonian, (17) having no spin-dependent terms, does not affect the spin-symmetry of the wave function. Hence, in what follows we restrict our discussion on the spatial part of the wave function $\Psi(x, y, t)$.

3.1.2 *Solving the time-dependent Schrödinger equation*

The TDSE with the Hamiltonian (17) is solved on a two-dimensional numerical grid with electron coordinates x and y. The numerical grid is shown in Fig. 4. The detailed numerical implementation of the TDSE is described in [32]. The grid is divided into various regions which

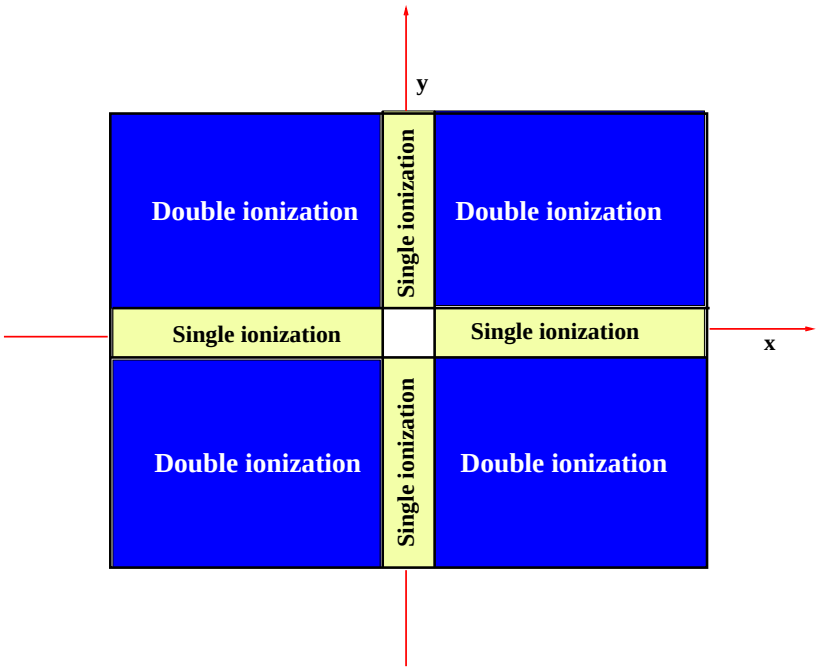

Figure 4: Schematic illustration of the numerical grid. Also shown are the demarcated regions which separate the bound state atom (white region) from the ionized atom (as labelled).

demarcate the bound state atom from the singly and the doubly ionized atom. In the white box region, both the electrons are close to the nucleus at the origin thus describing the neutral Helium atom. In the yellow regions one of the electron is far from the nucleus while the second one is still close to it. Hence probability density in this region describes He^{+}. In the blue regions both the electrons are far from the nucleus. Probability density in this region describes He^{++}.

The solution of the TDSE requires an initial state which is usually the ground state or another eigenstate of the Hamiltonian (18). The ground state is obtained via imaginary time-propagation. Excited states are calculated via Gram-Schmidt orthogonalization (see appendix A). In order to obtain the quasi-bound states such as the doubly excited states discussed in Chapter 6, the orthogonalization procedure is not practical. To obtain such states we use the spectral method [33] (see appendix B).

The computed initial wave function is always normalized on the grid. The norm $N(t)$ is defined as $N(t) = \langle \Psi(t) | \Psi(t) \rangle$. Once the initial state

is computed it is propagated in the presence of external laser fields according to the Hamiltonian (17),

$$\Psi(x,y,\Delta t) = \exp(-\mathrm{i}\hat{H}(t+\Delta t/2)\Delta t)\Psi(x,y,0). \tag{23}$$

The propagator $\exp(-\mathrm{i}\hat{H}\Delta t)$ is unitary, hence the norm is always conserved. Numerically, the propagator is approximated employing the Crank-Nicolson method. The details can be found in [32]. The finite size of the numerical grid imposes a practical limit to the unitarity of the propagation as absorbing boundaries are employed to absorb the density reaching the boundary. Due to this the norm, $N(t)$ of the wave function decreases. This can be used as a measure of the total ionization probability.

3.1.3 *Time-dependent observables*

The TDSE wave function $|\Psi(t)\rangle$ contains all the time-dependent information about the system under consideration. Observables are constructed from it to extract the information, such as multiple ionization probabilities $P^{n+}(t)$, the expectation value for an observable ($\langle x\rangle$, $\langle y\rangle$) and the photo-electron spectrum $\sigma(\mathcal{E})$. Here $n+$ refers to the n-fold ionized state of the atom, and $\mathcal{E}$ is the photo-electron energy. The ionization probabilities are defined in the following.

The total ionization probability $P(t)$ is defined as

$$P(t) = 1 - N(t). \tag{24}$$

The probabilities for bound state, singly and doubly ionized states are defined, respectively, as

$$\begin{aligned} P^{0}(t) &= \int\int_{\mathcal{A}(\mathrm{white-region})} dxdy\ |\Psi(x,y,t)|^2, \\ P^{1+}(t) &= \int\int_{\mathcal{A}(\mathrm{yellow-region})} dxdy\ |\Psi(x,y,t)|^2, \\ P^{2+}(t) &= \int\int_{\mathcal{A}(\mathrm{blue-region})} dxdy\ |\Psi(x,y,t)|^2. \end{aligned} \tag{25}$$

The expectation value for an operator $\hat{\mathcal{O}}$ is defined as

$$\langle\mathcal{O}\rangle = \int\int dxdy\ \Psi^*(x,y,t)\hat{\mathcal{O}}\Psi(x,y,t). \tag{26}$$

The expectation value of an operator can be experimentally measured. Of particular interest are photo-electron energy spectra (formally expectation values of projection operators on energy eigenstates). To obtain a photo-electron spectrum after the atom has been exposed to a laser pulse, the wave function $\Psi(x, y, T_{\text{end}})$ is stored. This wave function is then propagated with the unperturbed Hamiltonian (18), for a long time interval ($t_f - T_{\text{end}} \approx \mathcal{O}(1000)$) and the autocorrelation function

$$C(t) = \langle \Psi(T_{\text{end}}) | \Psi(t) \rangle \tag{27}$$

is computed [34].

The real-part of the Fourier transform of the autocorrelation function gives the photo-electron spectrum

$$\sigma(\mathcal{E}) = \frac{1}{\pi} \text{Re} \int_{T_{\text{end}}}^{t_f} C(t) e^{\text{i}\mathcal{E}(t - T_{\text{end}})} dt. \tag{28}$$

Apart from the observables shown here others can also be constructed depending upon the information required from the wave function, $\Psi(x, y, t)$.

3.1.4 *Linear Response Spectrum*

Consider the unperturbed Hamiltonian (18). The free evolution of the wavefunction would be

$$\Psi(x, y, t) = e^{-\text{i}\mathcal{E}_0 t} \Psi(x, y, 0). \tag{29}$$

With a delta kick-like electric field, the Hamiltonian (17) becomes

$$\hat{H}_{\text{kick}} = \hat{H}_0 - x\delta(t) - y\delta(t). \tag{30}$$

The solution of the TDSE then reads

$$\Psi(x, y, t) = e^{-\text{i}\mathcal{E}_0 t} \Psi(x, y, 0) + \sum_{j \neq 0} a_j e^{-\text{i}\mathcal{E}_j t} \Psi_j(x, y, 0). \tag{31}$$

Here, $\Psi_j(x, y, 0)$ is an excited state of the unperturbed Schrödinger equation (20) and a_j are coefficients whose detailed values are not relevant for what follows. The dipole expectation value after the kick is

$$\langle \Psi(t) | x + y | \Psi(t) \rangle = \int \int dx dy \Psi^*(x, y, t)(x + y) \Psi(x, y, t). \tag{32}$$

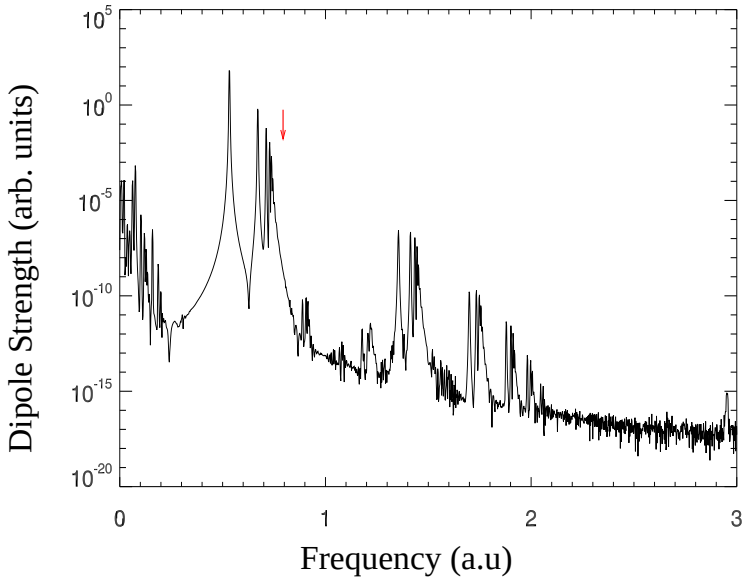

Figure 5: Linear response spectrum of model Helium atom obtained from the TDSE. The vertical arrow indicates the single-ionization threshold.

Substituting Eq. 31 in Eq. 32 it is clear that the Fourier transform of the dipole exhibits peaks at the energy difference between the unperturbed ground and the excited states.

As an example we consider $Z = 2$. The ground state energy for this system is, $\mathcal{E}_g = -2.238$ and the first excited spin-singlet state has the energy $\mathcal{E}_e = -1.705$. The linear response spectrum is plotted in Fig. 5. The arrow represents the single ionization threshold. The first peak represents the transition energy to the first excited spin-singlet state, $\omega_{\text{ge}} = \mathcal{E}_e - \mathcal{E}_g = 0.533$.

Since the ground state energy of the system is known, from the computed excitations we can infer the level scheme for the spin-singlet model Helium atom. This is shown in Fig.6.

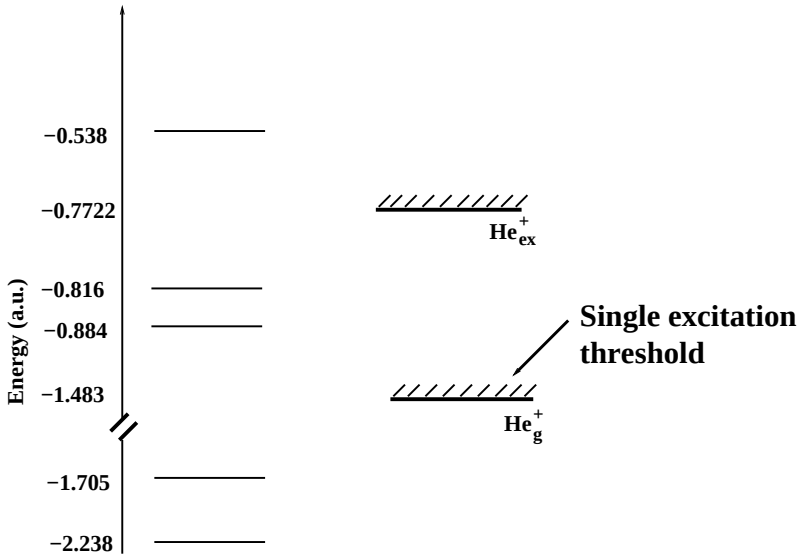

Figure 6: Level scheme for the model spin-singlet Helium atom obtained from the TDSE (not all spin-singlet states are shown). The doubly excited states occur above the ionization threshold for the singly excited states ($\mathcal{E} = -1.483$).

3.1.5 *Rabi Oscillations*

Consider the spin-singlet ground state and the first spin-singlet excited state for our model system. If we ignore all other states, we can recast the Hamiltonian (17) as a Hamiltonian of a two level system [35],

$$\hat{H}(t) = \hat{H}_0 + \hat{W}(x, y, t) = \mathcal{E}_g |g\rangle\langle g| + \mathcal{E}_e |e\rangle\langle e| + (x + y)E(t). \tag{33}$$

Here, $|g\rangle$ is the spin-singlet ground state whose energy is $\mathcal{E}_g$ and $|e\rangle$ is the spin-singlet excited state whose energy is $\mathcal{E}_e$.

Let their energy difference be denoted by ω_{ge}. Starting from the ground state, a low intensity laser pulse with frequency ω_1 is applied. The time-dependent wave function $|\Psi(t)\rangle$ in terms of $|g\rangle$ and $|e\rangle$ reads,

$$|\Psi(t)\rangle = c_g e^{-\mathrm{i}\mathcal{E}_g t}|g\rangle + c_e e^{-\mathrm{i}\mathcal{E}_e t}|e\rangle. \tag{34}$$

Plugging this ansatz into the TDSE governed by the Hamiltonian (33) leads upon multiplication from the left by $\langle g|$ and $\langle e|$ to

$$\begin{aligned} \mathrm{i}\frac{\partial}{\partial t}c_g(t) &= -\frac{1}{2}\hat{E}e^{\mathrm{i}(\omega_1-\omega_{\mathrm{ge}})t}c_e\langle g|x+y|e\rangle \\ \mathrm{i}\frac{\partial}{\partial t}c_e(t) &= -\frac{1}{2}\hat{E}e^{-\mathrm{i}(\omega_1-\omega_{\mathrm{ge}})t}c_g\langle e|x+y|g\rangle. \end{aligned} \tag{35}$$

$\langle g|x+y|e\rangle$ can be written as $\Omega_R e^{\mathrm{i}\gamma}$ where Ω_R is the Rabi-frequency. Here we have made use of the orthogonality of $|g\rangle$ and $|e\rangle$ and have neglected the fast rotating terms $\sim e^{\pm\mathrm{i}(\omega_1+\omega_{\mathrm{ge}})t}$ (rotating wave approximation). Subject to the initial conditions that at $t = 0$ only the ground state is populated we have $c_e(0) = 0$ and $c_g(0) = 1$. In this case the solution of the coupled equations (35) when $\omega_1 = \omega_{\mathrm{ge}}$ is

$$\begin{aligned} c_g(t) &= \cos(\frac{\Omega_R t}{2}), \\ c_e(t) &= \mathrm{i}e^{\mathrm{i}\gamma}\sin(\frac{\Omega_R t}{2}). \end{aligned} \tag{36}$$

If the pulse duration T_{end} is chosen such that $\Omega_R T_{\mathrm{end}} = \pi/2$ we end up having equal superposition of the ground and the excited state. Such a pulse is referred to as a $\pi/2-$pulse. On the other hand if T_{end} is chosen such that $\Omega_R T_{\mathrm{end}} = \pi$ we end up having all the population in the excited state. Such a pulse is referred to as a $\pi-$pulse. These pulses are employed experimentally to prepare the system in the desired state. The pulses applied should be of low intensity as low intensity ensures that the AC Stark shift of the atomic levels can be ignored.

As an example consider the model Helium atom with $Z = 2$. From the linear response spectrum Fig. 5 we find that the resonant frequency between the ground spin-singlet and the first excited spin-singlet is 0.533. We use a trapezoidal laser pulse with 2 cycles ramp up and then held constant with $\hat{E} = 0.0066$, $\omega_1 = 0.533$. At half Rabi-period $\pi/\Omega_R \approx 420$ the excited state is maximally populated and at full Rabi-period $\pi/\Omega_R \approx 840$ the ground state is maximally populated. In Fig. 7 we plot the population of the ground ($|c_g(t)|^2$) and the excited state ($|c_e(t)|^2$) together with the probability densities at half and full Rabi cycle. We see that at half Rabi cycle the first excited spin-singlet state is maximally populated while at full Rabi cycle the spin-singlet ground state is maximally populated.

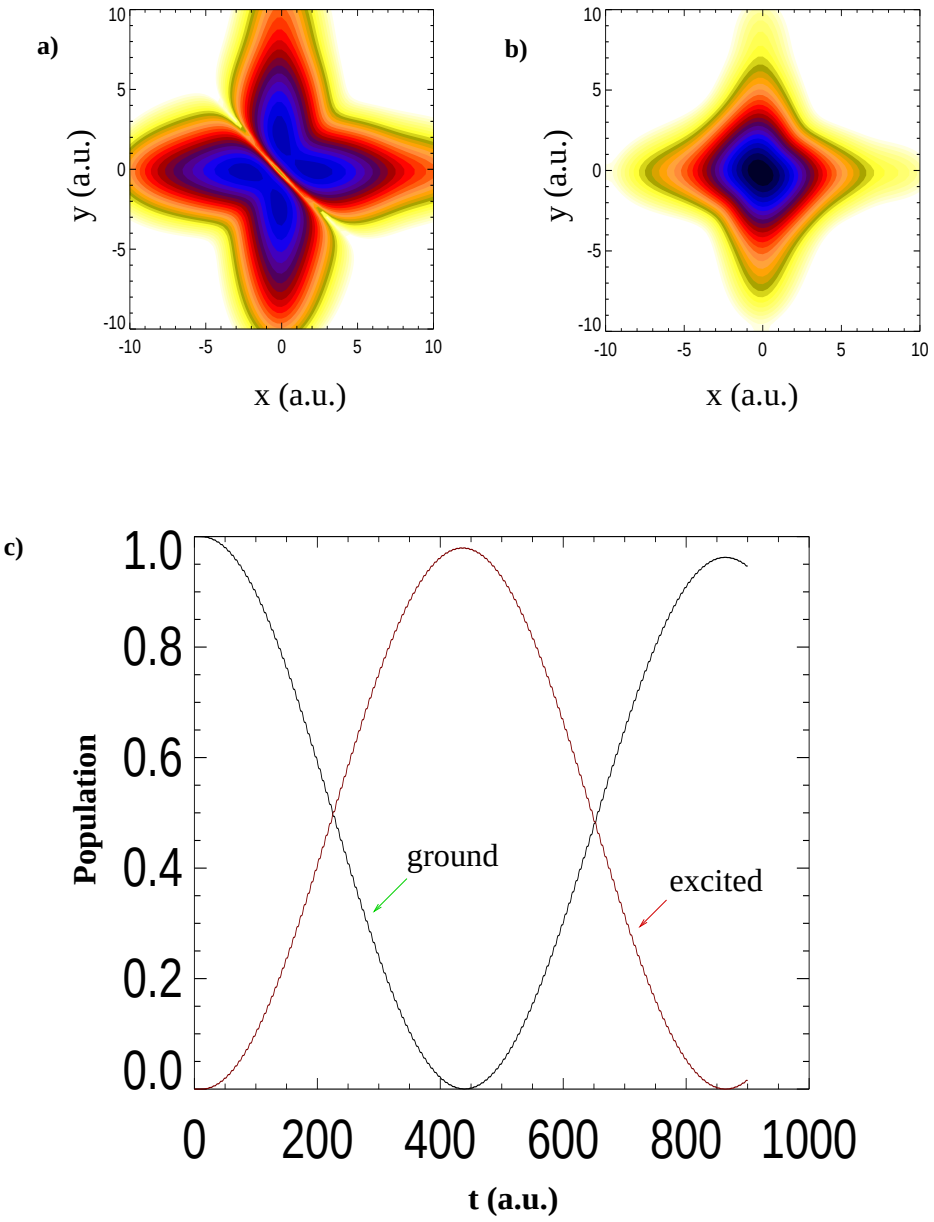

Figure 7: a) Probability density at $t = 420$ (half Rabi cycle), b) probability density at $t = 840$ (full Rabi cycle), c) population curves for a resonant interaction between the spin-singlet ground and the first spin-singlet excited state. Laser parameters specified in the text.

3.2 FLOQUET THEORY

Although the Floquet theory applies to any system with a time-periodic Hamiltonian let us specialize on the above introduced two electron system with electron coordinates x and y in a laser field $E(t)$ of frequency ω_1 in dipole approximation. The Hamiltonian in length gauge is given in (17).

For sufficiently long pulses

$$E(t+T) = E(t), \qquad T = \frac{2\pi}{\omega_1} \tag{37}$$

holds to high accuracy, and thus also $\hat{W}(t+T) = \hat{W}(t)$ so that

$$\hat{H}(t+T) = \hat{H}(t). \tag{38}$$

The Floquet theorem [1–4] states that in this case the TDSE corresponding to the Hamiltonian $\hat{H}$ has solutions of the form

$$\Psi(x,y,t) = \mathrm{e}^{-\mathrm{i}\epsilon t}\eta(x,y,t), \tag{39}$$

$\eta(x,y,t)$ being periodic itself,

$$\eta(x,y,t) = \eta(x,y,t+T). \tag{40}$$

ϵ is called the quasienergy. The wave functions $\eta(x,y,t)$ fulfill the following Schrödinger equation

$$\hat{\mathcal{H}}(t)\eta(x,y,t) = \epsilon\eta(x,y,t) \tag{41}$$

with

$$\hat{\mathcal{H}}(t) = \hat{H}(t) - \mathrm{i}\frac{\partial}{\partial t}. \tag{42}$$

If ϵ is an eigenvalue and $\eta(x,y,t)$ the corresponding eigenstate, also

$$\epsilon' = \epsilon + m\omega_1, \quad \eta'(x,y,t) = \mathrm{e}^{\mathrm{i}m\omega_1 t}\eta(x,y,t), \quad m \in \mathbb{Z} \tag{43}$$

are solutions of (41). Owing to the time periodicity of $\eta(x,y,t)$ we can expand

$$\eta(x,y,t) = \sum_n \zeta_n(x,y)\mathrm{e}^{-\mathrm{i}n\omega_1 t}. \tag{44}$$

For a monochromatic laser field the interaction Hamiltonian $\hat{W}(x,y,t)$ can be written as

$$\hat{W}(x,y,t) = \hat{W}^{+}(x,y)\exp(\mathrm{i}\omega_1 t) + \hat{W}^{-}(x,y)\exp(-\mathrm{i}\omega_1 t), \tag{45}$$

leading to the time-independent Floquet equation

$$\begin{aligned}(\epsilon + n\hbar\omega - \hat{H}_0)\zeta_n(x,y) \\ = \ \hat{W}^{+}(x,y)\zeta_{n-1}(x,y) + \hat{W}^{-}(x,y)\zeta_{n+1}(x,y).\end{aligned} \tag{46}$$

The index n of the Floquet state is known as the "block index," which may be interpreted as the number of photons involved in the process under study. Hence, the Floquet equation (46) couples any Floquet block n with its neighboring blocks $n \pm 1$ via absorption or emission of a photon, and thus, with help of the Floquet theorem the time-dependent problem of a quantum system in a time-periodic field has been reduced to an infinite set of coupled time-independent equations.

In principle, (46) is an infinite-dimensional matrix equation, in practice, it is truncated so that $n_{\mathrm{min}} \leq n \leq n_{\mathrm{max}}$. For obtaining the eigenvalue matrix equation (46), we implicitly assumed strict time-periodicity, which physically means that the laser pulse was always on—and will be on forever.

3.2.1 *Selection rules for high harmonic generation*

There are many ways to derive selection rules for harmonic generation. Most elegant, rigorous, and appropriate for our purpose is the approach employing dynamical symmetries [36, 37]. Consider the stationary Schrödinger equation (20). If the potential V is inversion-symmetric, $V(x,y) = V(-x,-y)$, the Hamiltonian $\hat{H}_0$ is invariant under spatial inversion as well,

$$\hat{P}_p f(x,y) = f(-x,-y), \quad \hat{P}_p^2 = 1, \ \hat{P}_p^{-1} = \hat{P}_p \tag{47}$$

$$[\hat{H}_0, \hat{P}_p] = 0, \tag{48}$$

so that for non-degenerate energies $\mathcal{E}$ the eigenstate $\Psi(x,y)$ is also an eigenstate of the spatial-inversion operator $\hat{P}_p$. Because of $\hat{P}_p^2 = 1$ the eigenvalues can only be ± 1 (parity):

$$\hat{P}_p \Psi(x,y) = \pm\Psi(x,y). \tag{49}$$

The full Hamiltonian (17) and the Floquet-Hamiltonian (42) are not invariant under spatial inversion but under the dynamical symmetry operation "spatial inversion combined with a translation in time by half a period",

$$[\hat{H}(t), \hat{P}_{pt}] = [\hat{\mathcal{H}}(t), \hat{P}_{pt}] = 0, \tag{50}$$

$$\hat{P}_{pt} f(x, y, t) = f(-x, -y, t + \pi/\omega_1), \qquad \hat{P}_{pt}^2 = 1, \tag{51}$$

$$\hat{P}_{pt} = \hat{P}_p \hat{P}_t = \hat{P}_t \hat{P}_p, \qquad \hat{P}_t f(x, y, t) = f(x, y, t + \pi/\omega_1). \tag{52}$$

For non-degenerate ϵ

$$\hat{P}_{pt} \eta(x, y, t) = \pm \eta(x, y, t). \tag{53}$$

Because of (44) we observe that

$$\hat{P}_{pt} \eta(x, y, t) = \sum_n (-1)^n \mathrm{e}^{-\mathrm{i}n\omega_1 t} \hat{P}_p \zeta_n(x, y), \tag{54}$$

and with (53) follows that

$$\hat{P}_p \zeta_n(x, y) = \pm (-1)^n \zeta_n(x, y), \tag{55}$$

i.e., the $\zeta_n(x, y)$ have an alternating parity with respect to the Floquet block index n.

The high harmonic spectrum $\sim \omega^4 |d(\omega)|^2$ is calculated via the Fourier-transformed dipole moment

$$d(\omega) \sim \int_{-\infty}^{\infty} \int_{-\infty}^{\infty} \Psi^*(x, y, t)(x + y)\Psi(x, y, t) \mathrm{e}^{\mathrm{i}\omega t} \, \mathrm{d}x \, \mathrm{d}y \, \mathrm{d}t. \tag{56}$$

Using (39) and (44), this can be written as

$$d(\omega) \sim \sum_{nm} \int \zeta_m^*(x, y)(x + y)\zeta_n(x, y) \, \mathrm{d}x \, \mathrm{d}y \int \mathrm{e}^{\mathrm{i}t[\omega - \omega_1(n-m)]} \, \mathrm{d}t. \tag{57}$$

The spatial integral is non-vanishing only if ζ_n has the opposite parity of ζ_m, i.e.,

$$n - m = 2k + 1, \qquad k \in \mathbb{Z}. \tag{58}$$

As a consequence, there will be harmonic peaks according

$$d(\omega) \sim \sum_{nk} \delta[\omega - \omega_1(2k + 1)] \int \zeta_{n-2k-1}^*(x, y)(x + y)\zeta_n(x, y) \, \mathrm{d}x \, \mathrm{d}y, \tag{59}$$

i.e., at positions

$$\omega = (2k+1)\omega_1. \tag{60}$$

This selection rule is the well-known result that an inversion-symmetric target in a linearly polarized laser field generates *odd* harmonics only. Note that the above derivation also holds for multi-electron targets because the electron-electron interaction is also invariant under the symmetry operations $\hat{P}_p$ and $\hat{P}_{pt}$.

3.2.2 *Superposition of Floquet states*

In the case of a non-adiabatic transfer of the field-free state to field-dressed states one has to allow for a superposition of Floquet states:

$$\Psi(x,y,t) = \sum_\beta \mathrm{e}^{-\mathrm{i}\epsilon_\beta t}\eta_\beta(x,y,t) = \sum_{\beta n} \mathrm{e}^{-\mathrm{i}t(\epsilon_\beta + n\omega_1)}\zeta_{\beta n}(x,y). \tag{61}$$

Note that $\eta_\beta(x,y,t)$ and $\zeta_{\beta n}(x)$ are not normalized because they carry the expansion coefficients.

Because of (61) the Fourier-transformed dipole will contain terms

$$\begin{aligned} d(\omega) \quad \sim \quad & \sum_{\beta\gamma nm} \int \zeta^*_{\gamma m}(x,y)(x+y)\zeta_{\beta n}(x,y)\,\mathrm{d}x\,\mathrm{d}y \\ & \times\delta[\omega - \omega_1(n-m) - (\epsilon_\beta - \epsilon_\gamma)]. \end{aligned} \tag{62}$$

Again, in order for the spatial integral to not vanish the parity of $\zeta_{\beta n}$ and $\zeta_{\gamma m}$ must be different. However, now this can be the case not only for $n - m = 2k+1$, but also for $n - m = 2k$ if the parity of, e.g., $\zeta_{\beta 0}$ is opposite to the one of $\zeta_{\gamma 0}$. Hence, one expects the peaks in the dipole spectrum at

$$\omega = k\omega_1 + \Delta\epsilon, \qquad k \in \mathbb{Z} \tag{63}$$

where $\Delta\epsilon = \epsilon_\beta - \epsilon_\gamma$ is the difference between two Floquet quasienergies. Thus besides odd harmonics even harmonics at $\omega = 2k\omega_1$ are observed if $\epsilon_\beta = \epsilon_\gamma$. Such a degeneracy between the (field-dressed) initial state and another one of opposite parity is also likely to populate the latter one.

3.3 DENSITY FUNCTIONAL THEORY

3.3.1 *Hohenberg-Kohn theorem*

The Hohenberg-Kohn (HK) [5,6] theorem states that all the ground state properties of a many-body system are determined by the single-particle probability density of the system. For an N-electron system (11) the single-particle probability density of the electronic ground state is

$$n_g(\mathbf{r}) = N \sum_{\sigma_1 \cdots \sigma_N} \int \mathrm{d}\mathbf{r}_2 \cdots \int \mathrm{d}\mathbf{r}_N |\Psi_0(\mathbf{r}\sigma_1 \cdots \mathbf{r}_N\sigma_N)|^2. \tag{64}$$

Here, Ψ_0 is the ground state of the stationary Schrödinger equation (20). The Hohenberg-Kohn theorem states

> In a finite, interacting N-particle system with a given particle-particle interaction there exists a one-to-one correspondence between the external potential $v(\mathbf{r})$ and the ground-state density $n_g(\mathbf{r})$. This implies that the external potential is a unique functional of the ground-state density $v[n_g](\mathbf{r})$ up to an arbitrary additive constant.

The statement is proven in [5]. For atomic systems with Coulombic interaction it is intuitive to see why this would be the case. The position of the nucleus for atoms is indicated by a cusp in the electronic ground-state density $n_g(x)$. The slope of the density at the cusp determines the nuclear charge [38]. The total number of electrons in the system is given by the integral over the single-particle density. This information completely determines the potential [7]. The potential then is a functional of the ground state density, as the theorem requires. This argument also holds true for molecular systems where instead of having just one cusp we have multiple cusps indicating the positions of the nuclei. The slope at each cusp then determines the nuclear charge. Hence from the ground state density alone one can construct the Hamiltonian of the system.

In order to formally find the ground state energy of the system, a constrained search formalism has been developed [6]. This formalism is an extension of the Rayleigh-Ritz principle of quantum mechanics which

states that the ground state energy $\mathcal{E}_g$ for the Hamiltonian (11) for an N-particle system is given by

$$\mathcal{E}_g = \min_\Psi \langle \Psi | \hat{H} | \Psi \rangle. \tag{65}$$

The constrained search for $|\Psi\rangle$ can be carried out in two steps, first by searching for those $|\Psi\rangle$ which produce a given single particle density $n(x)$ and then determine the density which yields the lowest energy. This can be summarized as

$$\mathcal{E}_0 = \min_n \left\{ \min_{\Psi \to n} \langle \Psi | \hat{H} | \Psi \rangle \right\}. \tag{66}$$

The object inside the parenthesis is the energy functional and can be written as

$$\begin{aligned} \mathcal{E}_v[n] &= \min_{\Psi \to n} \langle \Psi | \hat{H} | \Psi \rangle \\ &= \langle \Psi[n] | \hat{H} | \Psi[n] \rangle. \end{aligned} \tag{67}$$

Here, $|\Psi[n]\rangle$ is the unique wave function which produces the density n. Another universal functional can be defined if the Hamiltonian is written in terms of the kinetic and the potential energy operators (11) as

$$\mathcal{E}_v[n] = \langle \Psi[n] | \hat{T} + \hat{V}_{\text{ee}} + \hat{V} | \Psi[n] \rangle. \tag{68}$$

Then one can define a universal functional $F[n]$ as

$$\begin{aligned} F[n] &= \langle \Psi[n] | \hat{T} + \hat{V}_{\text{ee}} | \Psi[n] \rangle \\ &= \hat{T}[n] + \hat{V}_{\text{ee}}[n]. \end{aligned} \tag{69}$$

Here we have defined the interacting kinetic energy and the electron-electron interaction functional $\hat{T}[n]$ and $\hat{V}_{\text{ee}}[n]$, respectively. The energy functional then reads

$$\mathcal{E}_v[n] = \hat{T}[n] + \hat{V}_{\text{ee}}[n] + \int \mathrm{d}\mathbf{r}\, n(\mathbf{r}) v(\mathbf{r}). \tag{70}$$

Here v is the time-independent external potential defined in 14. The functional $F[n]$ is universal as it is the same for any N-electron system with the same electron-electron interaction, irrespective of the external potential acting on it.

3.3.2 *Kohn-Sham equation*

Let us assume that for an interacting system with a single particle ground state density n_g there exists a non-interacting system with the same ground state density. We write the non-degenerate ground state as a Slater determinant of orbitals Φ_i which satisfy the following equation

$$\left[-\frac{1}{2}\nabla^2 + v_{\mathrm{KS}}(\mathbf{r})\right]\Phi_i(\mathbf{r}) = \epsilon_i\Phi_i(\mathbf{r}), \tag{71}$$

with

$$\sum_{i=1}^{N}|\Phi_i(\mathbf{r})|^2 = n(\mathbf{r}). \tag{72}$$

v_{KS} is the Kohn-Sham potential which ensures that the ground state density for the non-interacting system is the same as the interacting one. The HK theorem for the Kohn-Sham system states that there is a one to one correspondence between the potential v_{KS} and the density n it generates. The kinetic energy and the total energy functional for the non-interacting system in terms of the orbitals Φ_i read

$$\begin{aligned}\hat{T}_{\mathrm{KS}}[n] &= \sum_{i=1}^{N} -\frac{1}{2}\int \Phi_i^*(\mathbf{r})\nabla^2\Phi_i(\mathbf{r})\mathrm{d}\mathbf{r} \\ \mathcal{E}_{v_{\mathrm{KS}}}[n] &= \hat{T}_{\mathrm{KS}}[n] + \int n(\mathbf{r})v_{\mathrm{KS}}(\mathbf{r})\mathrm{d}\mathbf{r}.\end{aligned} \tag{73}$$

We define the exchange-correlation energy functional as

$$\mathcal{E}_{\mathrm{XC}}[n] = F[n] - \frac{1}{2}\int\frac{n(\mathbf{r}_1)n(\mathbf{r}_2)}{|\mathbf{r}_1-\mathbf{r}_2|}\mathrm{d}\mathbf{r}_1\mathrm{d}\mathbf{r}_2 - \hat{T}_{\mathrm{KS}}[n]. \tag{74}$$

The ground state density of the system is obtained via the functional derivative of (74) with respect to the density with the constraint that the density integrates to the number of electrons. This reads

$$\frac{\delta}{\delta n(\mathbf{r})}\left[\mathcal{E}_{v_{\mathrm{KS}}}[n] - \mu_s\int n(\mathbf{r})\mathrm{d}\mathbf{r}\right] = \frac{\delta\hat{T}_{\mathrm{KS}}[n]}{\delta n(\mathbf{r})}[n] + v_{\mathrm{KS}}(\mathbf{r}) - \mu_s = 0. \tag{75}$$

For the interacting system the functional derivative of (70) employing (74) gives the following equation

$$\begin{aligned}&\frac{\delta}{\delta n(\mathbf{r})}\left[\mathcal{E}_v[n] - \mu\int n(\mathbf{r})\mathrm{d}\mathbf{r}\right] = \\ =\ &\frac{\delta\hat{T}_{\mathrm{KS}}[n]}{\delta n(\mathbf{r})}[n] + v(\mathbf{r}) + \int\frac{n(\mathbf{r}')}{|\mathbf{r}-\mathbf{r}'|}\mathrm{d}\mathbf{r}' + \frac{\delta\mathcal{E}_{\mathrm{XC}}[n]}{\delta n(\mathbf{r})}[n] - \mu = 0.\end{aligned} \tag{76}$$

Comparing Eq. (75) with Eq. (76) we find that if the interacting and the non-interacting system are solved for the same density n then we have constructed the potential v_{KS} which reads

$$v_{\mathrm{KS}}(\mathbf{r}) = v(\mathbf{r}) + \int \frac{n(\mathbf{r}')}{|\mathbf{r}-\mathbf{r}'|}\mathrm{d}\mathbf{r}' + \frac{\delta \mathcal{E}_{\mathrm{XC}}(\mathbf{r})}{\delta n(\mathbf{r})}[n]. \tag{77}$$

We now define an exchange-correlation potential v_{XC} as

$$v_{\mathrm{XC}}(\mathbf{r})[n] = \frac{\delta \mathcal{E}_{\mathrm{XC}}(\mathbf{r})}{\delta n(\mathbf{r})}[n]. \tag{78}$$

The ground state density can be computed via the following equation, also referred to as the Kohn Sham equation,

$$\left[-\frac{1}{2}\nabla^2 + v(\mathbf{r}) + \int \frac{n(\mathbf{r}')}{|\mathbf{r}-\mathbf{r}'|}\mathrm{d}\mathbf{r}' + v_{\mathrm{XC}}(\mathbf{r})[n]\right]\Phi_i(\mathbf{r}) = \epsilon_i \Phi_i(\mathbf{r}), \tag{79}$$

subject to the condition (72).

Hence to obtain ground state properties of an interacting system one can solve a non-interacting system instead which has the same single particle density as that of the interacting system. The HK theorem guarantees a one to one correspondence between the density and the potential that generates such a density. In practise, the task of obtaining the exact single particle ground state is reduced to finding good approximations for v_{XC} as this is an unknown *a priori*. This term contains all the many-body effects and is approximated by certain physical considerations of the problem, like the correct asymptotic behavior of the total potential. There are rungs of approximations in DFT to approximate the potential v_{XC}. The first rung is the local density approximation (LDA) [6, 7]. In this approximation one assumes that the exchange-correlation energy is that of a homogeneous electron gas, evaluated at the local density. The energy density of a homogeneous electron liquid as a function of local density $\sim n^{4/3}(\mathbf{r})$ and so $v_{\mathrm{XC}} \sim n^{1/3}(\mathbf{r})$. This approximation becomes more accurate the smaller the density gradients,

$$\frac{\nabla n(\mathbf{r})}{n(\mathbf{r})} \ll k_F(\mathbf{r}), \tag{80}$$

where $k_F(\mathbf{r})$ is the local Fermi wavevector. This condition is violated especially near the nuclei. Binding energies are typically too low in LDA.

The obtained values are still quite close to the actual values, lying within 5% of the actual ones. The drawback of this approximation is that it does not reproduce the correct asymptotic behavior of $v_{\mathrm{XC}}(\mathbf{r})$. For large distances $v_{\mathrm{XC}}(\mathbf{r})$ falls off exponentially with r rather than exhibiting a $1/r$ behavior. Despite its shortcomings it is one of the most widely used approximations.

The next rung on the ladder of approximations is occupied by generalized gradient approximation (GGA). In this approximation the potential $v_{\mathrm{XC}}(\mathbf{r})$ is a functional not just of the density but also of the gradient of the density. Even though this is appealing and seems as an improvement over LDA, in practise the obtained energies do not show a marked improvement in the accuracy and in some cases are even worse than those obtained by LDA [6, 7]. Succeeding rungs of approximations include additional elements like the Laplacian of the density and so on. For a thorough review of the taxonomy of the existing exchange-correlation functionals see, e.g., [6, 7]. For the purposes of this thesis such approximations are not essential as we construct the exact functionals with the aid of exactly solvable model systems discussed before in Section 3.1.1.

3.3.3 *Runge-Gross and van Leeuwen theorem*

After the ground state DFT was established on a firm footing, efforts were made to extend the theory for time-dependent external potentials. Unlike the ground state DFT, which is based on a minimization principle, the Runge-Gross (RG) [7, 10] and van Leeuwen theorem are based on the local force equations of quantum mechanics [11, 12].

The RG theorem states

> Starting from a given initial many-body state $\Psi_0(\mathbf{r})$ at time t_0, under the action of two different Taylor expandable external potentials $v(\mathbf{r}, t)$ and $v(\mathbf{r}', t) \neq v(\mathbf{r}, t) + c(t)$, the evolved densities will start to become different for $t > t_0$. Hence for a fixed initial many-body state there is a one to one correspondence between the density and the external potential.

For practical applications a time-dependent analogue of the KS equation is needed. The single particle density of the time-dependent interacting

system has to be reproduced by a non-interacting auxiliary system. That this is possible has been proven by van Leeuwen [7, 11]:

> For a given time-dependent density $n(\mathbf{r}, t)$ of a many-body system with a particle interaction $v_{ee}(\mathbf{r})$, initial state $\Psi_0(\mathbf{r})$ and an external time-dependent potential $v(\mathbf{r}, t)$ there exists another many-body system with a different particle interaction $v'_{ee}(\mathbf{r})$ and a unique Taylor expandable external potential $v'(\mathbf{r}, t)$ which reproduces the same time-dependent density as the previous system. The initial state $\Psi'_0(\mathbf{r})$ in this system must be chosen such that it correctly yields the given density and its time derivative at the initial time.

3.3.4 *Time-dependent Kohn-Sham equation*

In order to obtain the time evolution of the initially occupied orbitals $\Phi_i(\mathbf{r})$ under the action of a time-dependent external potential $v(\mathbf{r}, t)$ we require the orbitals to satisfy the time-dependent Kohn-Sham equation

$$\left[-\frac{1}{2}\nabla^2 + v_{KS}(\mathbf{r}, t)[n]\right] \Phi_i(\mathbf{r}, t) = \mathrm{i}\frac{\partial}{\partial t}\Phi_i(\mathbf{r}, t), \tag{81}$$

with time-dependent density

$$n(\mathbf{r}, t) = \sum_{i=1}^{N} |\Phi_i(\mathbf{r}, t)|^2, \tag{82}$$

and

with the initial condition

$$\Phi_i(\mathbf{r}, t_0) = \Phi_i(\mathbf{r}). \tag{83}$$

The initial condition implies that only initially occupied orbitals are propagated via Eq. (81). The effective potential in Eq. (81) is given by

$$v_{KS}(\mathbf{r}, t)[n] = v(\mathbf{r}, t) + \int \frac{n(\mathbf{r}', t)}{|\mathbf{r} - \mathbf{r}'|}\mathrm{d}\mathbf{r}' + v_{XC}[n](\mathbf{r}, t). \tag{84}$$

The exchange-correlation potential also has to satisfy an initial condition which is

$$v_{XC}[n_0](\mathbf{r}, t_0) = v^0_{XC}[n_0](\mathbf{r}), \tag{85}$$

i.e. the time-dependent exchange correlation potential must match the static exchange-correlation potential at the initial time. This means that the exchange-correlation potential depends on the initial static orbitals $\Phi_i(\mathbf{r})$. The time-dependent exchange-correlation potential is a functional of the time-dependent density and the initial state of the interacting and the non-interacting system. This can be expressed by writing the exchange-correlation potential v_{XC} as

$$v_{\mathrm{XC}}[n](\mathbf{r},t) = v_{\mathrm{XC}}[n,\Phi_i(\mathbf{r}),\Psi_0(\mathbf{r})](\mathbf{r},t). \tag{86}$$

The task of making approximations for time-dependent exchange-correlation potentials is therefore even more tedious than building approximations for the static exchange-correlation potential.

3.3.5 *Exact orbitals and potentials*

Once we have obtained $\Psi(x,y,t)$ for a spin-singlet two electron system by solving the corresponding TDSE we can construct the exact KS orbital and the potential following Refs. [39,40]. In the two-electron spin-singlet case the KS wave function consists of only one spatial orbital $\Phi(x,t)$ i.e.,

$$\Phi(x\sigma_1,y\sigma_2,t) \;=\; \Phi(x,t)\Phi(y,t)\frac{1}{\sqrt{2}}\left(|\uparrow_1\rangle|\downarrow_2\rangle - |\downarrow_1\rangle|\uparrow_2\rangle\right). \tag{87}$$

The KS orbital can be written as

$$\Phi(x,t) = \sqrt{n(x,t)/2}\;\mathrm{e}^{\mathrm{i}S(x,t)}, \tag{88}$$

where $n(x,t)$ is the exact particle density and $S(x,t)$ is the exact phase of the KS orbital. The expression for the phase in terms of density is given by the continuity equation as [40,41]

$$-\partial_x\left[n(x,t)\partial_x S(x,t)\right] = \partial_t n(x,t). \tag{89}$$

The KS Hamiltonian for the two electron spin-singlet system is

$$\hat{H}_{\mathrm{KS}}([n];t) = -\frac{1}{2}\frac{\partial^2}{\partial x^2} + v_{\mathrm{KS}}([n];x,t). \tag{90}$$

The corresponding time-dependent KS equation is

$$\hat{H}_{\mathrm{KS}}\Phi(x,t) = \mathrm{i}\frac{\partial}{\partial t}\Phi(x,t). \tag{91}$$

The above equation can be inverted to write the KS potential in terms of the KS orbital as [40]

$$\begin{aligned} v_{\mathrm{KS}}(x,t) &= \frac{\mathrm{i}\partial_t\Phi(x,t) + \frac{1}{2}\partial_x^2\Phi(x,t)}{\Phi(x,t)} \\ &= \frac{1}{2}\frac{\partial_x^2\sqrt{n(x,t)}}{\sqrt{n(x,t)}} - \partial_t S(x,t) - \frac{1}{2}\left[\partial_x S(x,t)\right]^2. \end{aligned} \tag{92}$$

The imaginary part of the potential is zero due to the continuity equation (89). The density $n(x,t)$ and the phase $S(x,t)$ are computed from $\Psi(x,y,t)$ [39], and by the above construction we obtain the exact KS potential. Such a straightforward construction is possible only if we have a single spatial orbital. In the general case of several KS orbitals one would need to employ a computationally more demanding fixed-point method, as demonstrated in [42, 43]. In order to appreciate the need for construction of exact potentials and orbitals we would like to point out the open challenges in TDDFT that have been addressed via such an exact construction. The results have been fruitful as such a construction offers insight not accessible without an exact construction of the KS Hamiltonian. This is summarized in the following table along with the present status of the problem.

Present challenges of TDDFT addressed via an exact construction	Present status
Strong field double ionization in a model Helium atom.	This was investigated in [39]. It was found that incorporating the discontinuity of v_{XC} as the electron number deviates from an integer value improves the description of the ionization process. Also the observable functional for double ionization requires advanced approximations [13].
The theoretical controversy regarding applicability of Floquet theorem to TDDFT Hamiltonians.	The conditional nature of the applicability of the Floquet theorem to TDDFT Hamiltonians was demonstrated by us in [44] and will be discussed in this work in Chapter 5.
Description of the highly correlated process of autoionization within TDDFT.	Exact KS orbitals and potentials have been obtained and display the essential features which must be incorporated by any density functional to correctly reproduce the dynamics of autoionization. This forms a part of this work and will be discussed in Chapter 6.
Description of charge transfer dynamics within TDDFT.	It has been shown recently how charge transfer dynamics work in TDDFT using the construction for exact orbitals and potentials [45]. Essential features have been extracted and any density functional must have these features in order to reproduce the charge transfer dynamics correctly within TDDFT.

3.3.6 *Floquet formulation for time-dependent density functional theory*

TDDFT is in principle an exact alternative to solving the TDSE for the full many-body problem, thereby relieving us of the problem of the "exponential wall". It would be beneficial to have a Floquet formulation for the TDDFT as we have for the TDSE (see section 3.2). Such a formulation would reduce the task of solving the time-dependent KS equations to solving an infinite set of time-independent equations which can also be truncated in practice as seen in section 3.2 for the TDSE.

The non-interacting KS system, by construction, yields the same single-particle density $n(x,t)$ as the interacting system. For the model helium atom the KS Hamiltonian reads

$$\hat{H}_{\mathrm{KS}}([n];t) = -\frac{1}{2}\frac{\partial^2}{\partial x^2} + v_{\mathrm{KS}}([n];x,t), \tag{93}$$

We make the basic assumption of any Floquet approach in a density-functional framework: if the Hamiltonian $\hat{H}(t)$ describing the N interacting electrons is periodic with the frequency ω_1, i.e., $E(t+T) = E(t)$ with $T = 2\pi/\omega_1$, then we assume the same periodicity for the KS Hamiltonian as well. We neglect for the moment potential problems with respect to the non-linear nature of the KS equations, which will be discussed in detail in the subsequent Chapter 5 of this work.

If the KS Hamiltonian is periodic with T then, by virtue of the Floquet theorem, we can write the KS orbitals in a time-periodic (Floquet) basis $\{\phi_\alpha(x,t)\}_{\alpha\in\mathbb{N}}$ as

$$\Phi_k(x,t) = \sum_\alpha c_{k\alpha} \mathrm{e}^{-\mathrm{i}\xi_\alpha t}\phi_\alpha(x,t), \tag{94}$$

where the ξ_α are the so-called quasi-energies and $c_{k\alpha} = \langle\phi_\alpha(t=0)|\Phi_k(t=0)\rangle$. Further, the $\phi_\alpha(x,t)$ are periodic in T, i.e.,

$$\phi_\alpha(x,t) = \phi_\alpha(x,t+T). \tag{95}$$

The Floquet orbitals $\phi_\alpha(x,t)$ fulfill the eigenvalue equation

$$\hat{\mathcal{H}}(t)\phi_\alpha(x,t) = \xi_\alpha\phi_\alpha(x,t) \tag{96}$$

with

$$\hat{\mathcal{H}}(t) = \hat{H}_{\mathrm{KS}}([n];t) - \mathrm{i}\partial_t, \tag{97}$$

i.e., ξ_α assumes the role of an eigenvalue and $\phi_\alpha(x,t)$ is the corresponding eigenstate. If so, also

$$\xi'_\alpha = \xi_\alpha + m\omega_1, \quad \phi'_\alpha(x,t) = \mathrm{e}^{\mathrm{i}m\omega_1 t}\phi_\alpha(x,t), \quad m \in \mathbb{Z} \tag{98}$$

are solutions of the eigenvalue equation (96). Owing to the time periodicity of $\phi_\alpha(x,t)$ we can write

$$\phi_\alpha(x,t) = \sum_l \varphi_{\alpha,l}(x)\mathrm{e}^{-\mathrm{i}l\omega_1 t}, \qquad l \in \mathbb{Z}. \tag{99}$$

With Eqs. (94) and (99) the KS orbital can thus be written as,

$$\Phi_k(x,t) = \sum_{l\alpha} c_{k\alpha}\mathrm{e}^{-\mathrm{i}(\xi_\alpha + l\omega_1)t}\varphi_{\alpha,l}(x), \tag{100}$$

where the eigenstates $\{\varphi_{\alpha,l}(x)\}_{\alpha\in\mathbb{N},l\in\mathbb{Z}}$ form the time-independent Floquet basis.

We divide the Hamiltonian $\hat{H}_{\mathrm{KS}}([n];t)$ into a time-independent part

$$\hat{H}_0 = -\frac{1}{2}\frac{\partial^2}{\partial x^2} - \frac{Z}{\sqrt{x^2+\epsilon}}, \tag{101}$$

the coupling to the monochromatic external field

$$xE(t) = v^+(x)\mathrm{e}^{\mathrm{i}\omega_1 t} + v^-(x)\mathrm{e}^{-\mathrm{i}\omega_1 t}, \tag{102}$$

and $v_{\mathrm{Hxc}}([n];x,t)$. Since we tentatively assume time-periodicity of the whole KS Hamiltonian we can write

$$v_{\mathrm{Hxc}}([n];xt) = \sum_l \mathrm{e}^{-\mathrm{i}l\omega_1 t}\left[v_{\mathrm{Hxc}}([n];x)\right]_l, \tag{103}$$

$l \in \mathbb{Z}$. Plugging the expansions (99), (102), and (103) in Eq. (96) we obtain the TDDFT-Floquet equations [46]

$$\begin{aligned}(\xi_\alpha + l\omega_1 - \hat{H}_0)\varphi_{\alpha,l}(x) \\ = \; & v^+(x)\varphi_{\alpha,l-1}(x) + v^-(x)\varphi_{\alpha,l+1}(x) \\ + \; & \sum_m (v_{\mathrm{Hxc}}([n];x))_{l-m}(x)\varphi_{\alpha,m}(x).\end{aligned} \tag{104}$$

The Floquet equation (104) couples any Floquet block l to its neighboring blocks $l \pm 1$ via absorption or emission of a photon. Contributions

of non-neighboring blocks may only be included through the Fourier-components of the Hxc potential. This is different from the Floquet equations for the interacting TDSE (46) which couple only neighboring blocks because $E(t)$ is the only time-dependent element in the TDSE Hamiltonian. However, in the TDSE case the Floquet basis functions depend on all spatial variables, not just on a single one as in the KS case.

In principle, Eq. (104) is an infinite-dimensional set of coupled partial differential equations, in practice, it is truncated so that $l_{\min} \leq l \leq l_{\max}$ where $|l_{\min}|$ and $|l_{\max}|$ should be large enough to capture all the relevant processes in which photons are emitted or absorbed.

If Eq. (104) was valid, the periodic time-dependent many-body problem would be significantly simplified because the time-dependence had been eliminated via Floquet theory and the "exponential wall" via TDDFT.

4

FLOQUET ANALYSIS OF REAL-TIME WAVE FUNCTIONS

As many interesting phenomena such as the AC Stark effect, Rabi oscillations, or stabilization against ionization [47] is most conveniently analyzed in terms of light-induced states (LIS), it is desirable to extract the "Floquet information" from the real-time wave function "on-the-fly" while propagating (or by post-processing) it, without having to solve the Floquet equation as well. We present a method to analyze strong (i.e., non-perturbative) laser-driven quantum dynamics via the (time-resolved) Floquet information contained in the corresponding real-time wave function [48]. This method has been applied in [49] to study the role of the Kramers-Henneberger atom in the higher-order Kerr effect.

In this Chapter this method will be applied to a) understand the presence of even harmonics in the case of an inversion-symmetric potential with only one bound state, b) investigate how the population of Floquet states changes under (gauge) transformations, c) obtain an observable time-resolved Floquet spectra and d) interpret the channel-closing phenomenon and related spectral enhancements in terms of Floquet state-crossings.

The content of this chapter has been published in [48].

4.1 EVEN HARMONICS

It is known that high harmonic peaks at positions different from odd multiples of the fundamental laser frequency ω_1 are to be expected for an inversion-symmetric potential if at least two Floquet states of opposite parity are populated (see Sec. 3.2 or [50, 51]). Physically, the superposition of two Floquet states may amount to, e.g., the absorption of n photons of energy ω_1 but emission of one photon of energy $n\omega_1 - \Delta\epsilon$, with $\Delta\epsilon$ being the energy difference between initial and final state. This should lead to hyper-Raman lines in the spectra which, however, are typ-

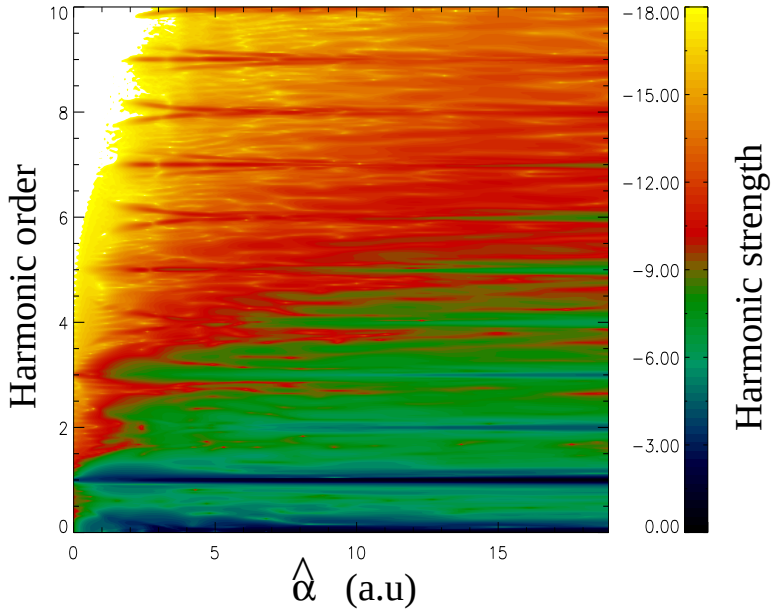

Figure 8: Logarithmically scaled harmonic generation strength $\omega^4|d(\omega)|^2$ vs harmonic order and excursion amplitude $\hat{\alpha}$ ($\omega_1 = 1$, vector potential $A(t)$ ramped up and down over 4 cycles and held constant for 30 cycles) [48].

ically weak [51,52]. Nevertheless, if they are observable, even harmonics are expected in the case of degeneracy, $\Delta\epsilon = 0$.

We consider an electron in the Pöschl-Teller potential

$$V(x) = -\frac{1}{\cosh^2(x)} \tag{105}$$

subject to a laser field. The potential (105) supports only a single bound state $\Psi_0(x)$ of energy $\mathcal{E}_0 = -0.5$. Hence, superpositions of field-free bound states are ruled-out. As a consequence, perturbation theory in the external field can certainly not predict hyper-Raman lines or even harmonics. However, Fig. 8 shows the logarithmically scaled harmonic generation strength $\omega^4|d(\omega)|^2$ as obtained from the numerical solution of the TDSE. The harmonic generation strength is plotted vs harmonic order ω/ω_1 and the amplitude $\hat{\alpha}$ of the excursion

$$\alpha(t) = \int^t A(t)\,\mathrm{d}t \tag{106}$$

with $A(t)$ the vector potential of the laser field. The electric field is given by $E(t) = -\partial_t A(t)$. The laser pulse parameters are specified in the figure caption. One sees that for sufficiently strong excursion amplitude $\hat{\alpha}$ even harmonics appear too. Picking an even harmonic at $\hat{\alpha} > 15$ (e.g., the 6th) and tracing it back to low $\hat{\alpha}$ reveals that the peak splits and rapidly drops in magnitude (e.g., around $\hat{\alpha} \simeq 2$ for the 6th harmonic). In the next Section we will use our real-time Floquet method to show that the appearance of even harmonics is due to the population of several LIS that become quasi-degenerate as $\hat{\alpha}$ increases.

4.2 Floquet state analysis of real-time wave functions

The extraction of Floquet information contained in the real-time wave function is useful to analyze any feature of interest in harmonic generation spectra. We start with the determination of the quasi-energy of the populated Floquet states. Once these energies are known the corresponding Floquet states can be obtained. The method is similar to the one proposed in [33] for field-free dynamics.

The numerical solution of the TDSE in real time yields $\Psi(x,t)$. As in the two-dimensional case (61) the wave function $\Psi(x,t)$ can be expanded as

$$\Psi(x,t) = \sum_{\beta n} \mathrm{e}^{-\mathrm{i}t(\epsilon_\beta + n\omega_1)} \zeta_{\beta n}(x). \tag{107}$$

Upon multiplication of (107) by an even or odd test function $q_\pm(x)$, spatial integration, and Fourier transformation,

$$Q_\pm(\mathcal{E}) = \sum_{\beta n} \int_{t_1}^{t_2} \mathrm{e}^{-\mathrm{i}t(\epsilon_\beta + n\omega_1 - \mathcal{E})} \mathrm{d}t \int q_\pm(x) \zeta_{\beta n}(x)\, \mathrm{d}x \tag{108}$$

one can extract the Floquet energies

$$\mathcal{E}_{\beta n} = \epsilon_\beta + n\omega_1 \tag{109}$$

belonging to even or odd Floquet states $\zeta_{\beta n}$, respectively. The even test function is, e.g., simply unity for all x, the odd test function may be chosen 1 for $x > 0$ and -1 for $x < 0$. The purpose of these test functions is to extract the even and odd-parity Floquet states, respectively. For an infinitely extended pulse one can extend t_1 to $-\infty$ and t_2 to $+\infty$. In finite pulses one can do a time-resolved study by integrating over a finite time interval around t. Of course, only the energies of the populated (and thus relevant) Floquet states $\zeta_{\beta n}$ can be determined via the positions of peaks of $|Q_\pm(\mathcal{E})|^2$.

To obtain the corresponding Floquet state we multiply the wave function (107) by $\exp(\mathrm{i}t\mathcal{E})$ and integrate over time, mainly the Floquet states $\zeta_\mathcal{E}$ for which the phase is stationary, i.e., $\mathcal{E} = \epsilon_\beta + n\omega_1$ "survive,"

$$\zeta_\mathcal{E}(x) \sim \int_{t_1}^{t_2} \mathrm{e}^{\mathrm{i}t\mathcal{E}} \Psi(x,t)\, \mathrm{d}t. \tag{110}$$

Here, we have proportionality only, because the right hand side gives some non-normalized wave function. The integration time $t_2 - t_1$ has to be sufficiently long in order to cover many oscillations of the wave function.

Starting from the ground state in the potential (105), we solved the TDSE for a high-frequency laser field of vector potential $A(t) = -\hat{A}(t) \sin \omega_1 t$ for $\omega_1 = 4$ and $\hat{A}(t)$ describing a trapezoidal pulse shape with up- and down-ramps over 4 cycles and 1200 cycles constant amplitude $\hat{A}$, denoted (4,1200,4). Figure 9 shows

$$R = |Q_+|^2 + |Q_-|^2 \tag{111}$$

(with the time-integral in (108) performed over the entire pulse) as a contour plot vs the excursion amplitude $\hat{\alpha} = \hat{A}/\omega_1$ and energy $\mathcal{E}$ for an energy interval within the zeroth Floquet block $n = 0$. Plotting $|Q_+|^2$ and $|Q_-|^2$ individually allows to distinguish the parity of the states (labeled 'even' or 'odd' in Fig. 9). For $\hat{\alpha} \to 0$ only the field-free state at $\mathcal{E} = -0.5$ remains. However, with increasing excursion amplitude $\hat{\alpha}$ light-induced quasi-bound states emerge, which are populated due to the finite rise-time of the laser field. From the populations (see color-coding) one infers that besides the field-dressed ground state around $\hat{\alpha} = 6$ the second excited field-dressed state is more populated than the first excited. For increasing $\hat{\alpha}$ the field-dressed ground state and the field-dressed first excited state become almost degenerate so that $\Delta\epsilon \to 0$ in (63), explaining the generation of even harmonics.

Using (110) we extracted field-dressed states. Figure 10 shows the field-dressed ground state for the Floquet blocks $n = 0$ (a) and $n = -1$ (b) for $\hat{\alpha} = 4$. The integration time was again the pulse duration. Equation (110) in general yields a complex wave function $\zeta_\mathcal{E} = \tilde{\zeta}_\mathcal{E} e^{i\theta}$. The plots in Fig. 10 show the real wave function $\tilde{\zeta}_\mathcal{E}$. It is seen that the parity indeed changes as one decreases n by one. For $n = 0$ and $\hat{\alpha} = 0$ the ground state must be even. Hence, for $n = -1$ it is odd, in accordance with (55).

It is known that if the laser frequency is tuned around resonances field-dressed states originating from different Floquet blocks (and corresponding to the coupled field-free states) display avoided crossings. These crossings have been shown to be related to localization, and to chaos in the corresponding classical system [53]. The separation of the two dressed states involved corresponds to the Rabi frequency and is proportional to the field strength of the driving laser. We will now show that the same is observed for transitions between dressed states, i.e., we use the laser of frequency ω_1 to dress the system and a second weaker laser of frequency $\tilde{\omega}$ to induce transitions between dressed states. The second laser will dress the already dressed system [54], and the "dressed^2" states (or two color-dressed states) should display avoided crossings as the frequency $\tilde{\omega}$ is tuned around the energy gap of two dressed states.

From Fig. 9 one infers that for an excursion amplitude, $\hat{\alpha} = 2.5$ the energy difference between the field-dressed ground state and the field-dressed first excited state is $\epsilon_1 - \epsilon_0 \simeq 0.155$. Hence, we tune the frequency $\tilde{\omega}$ of the second laser around this energy difference. The pulse envelope was the same for both lasers, and the electric field amplitude

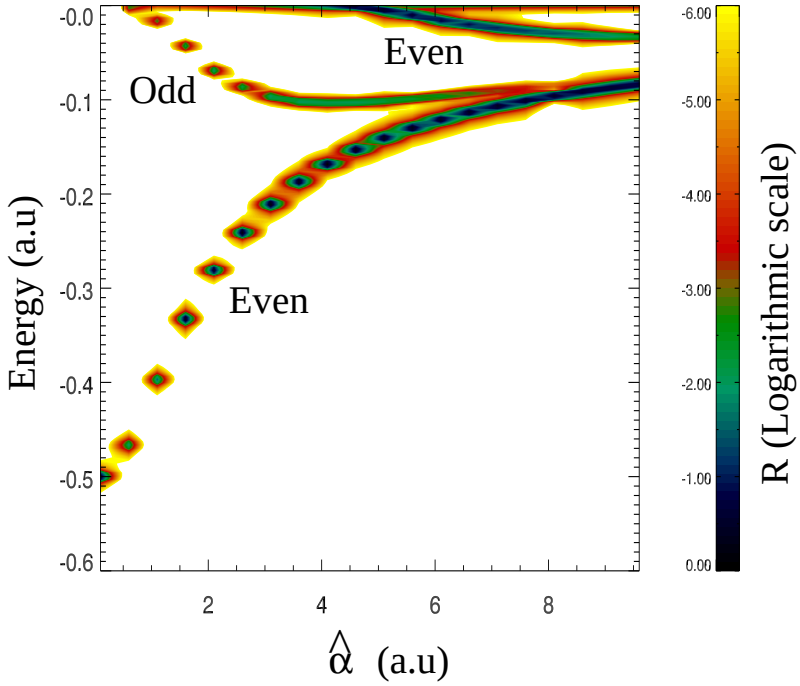

Figure 9: Logarithmic plot of $R = |Q_+|^2 + |Q_-|^2$ *vs* $\mathcal{E}$ and $\hat{\alpha} = \hat{A}/\omega_1$, showing the quasi-energies of the (populated) field-dressed states. The laser frequency was $\omega_1 = 4$. The pulse shape was trapezoidal (4,1200,4) in the vector potential of amplitude $\hat{A}$. For each $\hat{\alpha}$ the maximum in R was renormalized to unity [48].

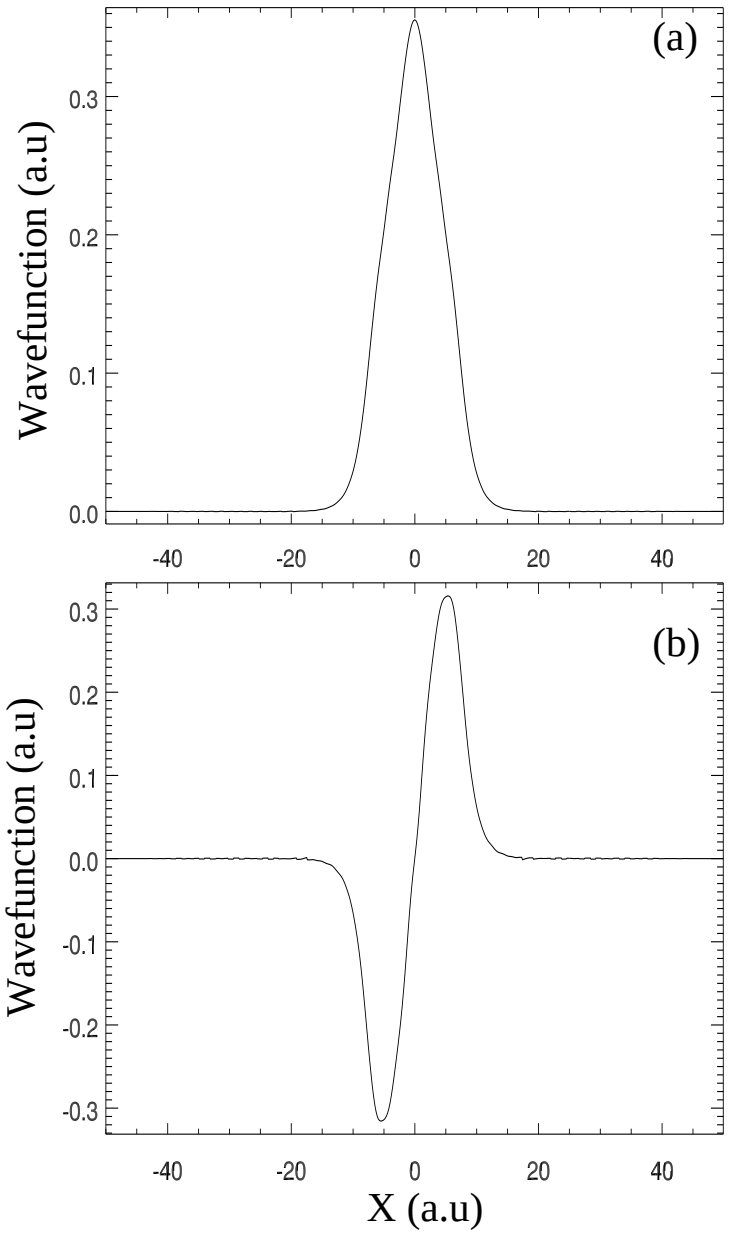

Figure 10: Field-dressed ground state wave function $\tilde{\zeta}_{0n}$ for $\hat{\alpha} = 4$. (a) Floquet block $n = 0$, (b) $n = -1$ [48].

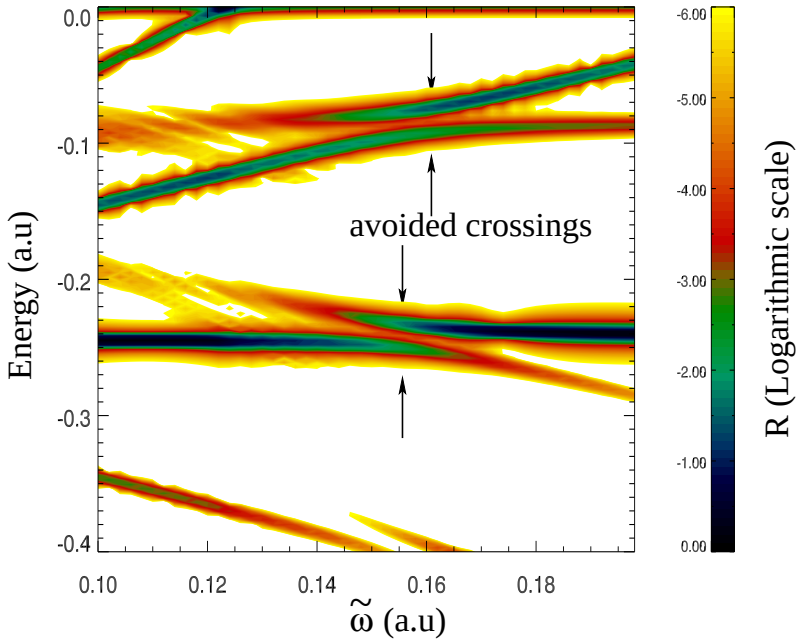

Figure 11: R *vs* energy $\mathcal{E}$ and second-laser frequency $\tilde{\omega}$ for first-laser $\hat{\alpha} = 2.5$ [48].

of the second laser was $\tilde{\hat{E}} = 0.01 = \tilde{\hat{A}}\tilde{\omega} = \tilde{\hat{\alpha}}\tilde{\omega}^2$ for all $\tilde{\omega}$. Figure 11 shows results for the Floquet energy spectrum R vs energy and $\tilde{\omega}$ for $\hat{\alpha} = 2.5$. If the two frequencies ω_1 and $\tilde{\omega}$ are incommensurate the Hamiltonian is not periodic at all. However, our approach does not require periodicity, and we expect a Floquet analysis to be meaningful as long as the two-color set-up is *approximately* periodic, namely in $\tilde{T} = 2\pi/\tilde{\omega}$ because $\omega_1 \gg \tilde{\omega}$. In fact, the avoided crossings of ϵ_0 with $\epsilon_1 - \tilde{\omega}$ and of $\epsilon_0 + \tilde{\omega}$ with ϵ_1 around $\tilde{\omega} = 0.155$ are clearly visible in Fig. 11.

4.3 Population of Floquet states in different gauges and frames

We consider transformations $\hat{G}(t)$ which are periodic in time and reduce to unity as the laser field goes to zero,

$$\hat{G}(t+T) = \hat{G}(t), \qquad \hat{G}(t)|_{\alpha,E,A=0} = \hat{1}. \tag{112}$$

Now, since each Floquet state η_β fulfills (41),

$$\hat{G}(t)\hat{\mathcal{H}}(t)\hat{G}^{-1}(t)\hat{G}(t)|\eta_\beta(t)\rangle = \hat{\mathcal{H}}'(t)|\eta'_\beta(t)\rangle = \epsilon_\beta|\eta'_\beta(t)\rangle \tag{113}$$

where $\hat{\mathcal{H}}'(t) = \hat{G}(t)\hat{\mathcal{H}}(t)\hat{G}^{-1}(t)$ is the transformed Floquet-Hamiltonian and $|\eta'_\beta(t)\rangle = \hat{G}(t)|\eta_\beta(t)\rangle$ the transformed Floquet state. The quasi-energy ϵ_β is not affected by the transformation, and $|\eta'_\beta(t)\rangle$ is also periodic because of (112), so that with (44)

$$\sum_n \mathrm{e}^{-\mathrm{i}n\omega_1 t}|\zeta'_{\beta n}\rangle = \sum_{nm} \mathrm{e}^{-\mathrm{i}(n+m)\omega_1 t}\hat{G}_m|\zeta_{\beta n}\rangle, \tag{114}$$

where $\hat{G}(t) = \sum_m \mathrm{e}^{-\mathrm{i}m\omega_1 t}\hat{G}_m$, and thus

$$|\zeta'_{\beta\ell}\rangle = \sum_n \hat{G}_{\ell-n}|\zeta_{\beta n}\rangle. \tag{115}$$

We now specialize on transformations $\hat{G}$ that commute with the dynamical symmetry operation $\hat{P}_{pt}$,

$$[\hat{G}(t), \hat{P}_{pt}] = 0. \tag{116}$$

Examples are gauge transformations, e.g., for the transformation from velocity gauge, where

$$\hat{W}(t) = \hat{p}A(t) + \frac{1}{2}A^2(t), \tag{117}$$

to the length gauge one has

$$G_{\mathrm{LG}}(t) = \exp\left[\mathrm{i}xA(t')\right]. \tag{118}$$

Another example is the Pauli-Fierz or Kramers-Hennenberger (KH) transformation. If we start from the velocity gauge interaction (117) the KH transformation reads

$$\hat{G}_{\mathrm{KH}}(t) = \exp\left[\frac{\mathrm{i}}{2}\int_\infty^t A^2(t')\,\mathrm{d}t' + \mathrm{i}\alpha(t)\hat{p}\right]. \tag{119}$$

This amounts to a translation in position space by the free electron excursion $\alpha(t)$ and a trivial (purely time-dependent) contact transformation. The KH Floquet-Hamiltonian is

$$\hat{\mathcal{H}}'(t) = \hat{\mathcal{H}}_{\mathrm{KH}}(t) = \frac{1}{2}\hat{p}^2 + V[x + \alpha(t)] - \mathrm{i}\frac{\partial}{\partial t}. \tag{120}$$

As a consequence of (116),

$$\hat{P}_{pt}|\eta'_\beta(t)\rangle = \hat{G}(t)\hat{P}_{pt}|\eta_\beta(t)\rangle = \pm|\eta'_\beta(t)\rangle \tag{121}$$

with the eigenvalue ± 1 the same as for $\hat{P}_{pt}|\eta_\beta(t)\rangle = \pm|\eta_\beta(t)\rangle$. One also finds $\hat{G}_m = (-1)^m \hat{P}_p \hat{G}_m \hat{P}_p$ and $\hat{P}_p|\zeta'_{\beta\ell}\rangle = \pm(-1)^\ell|\zeta'_{\beta\ell}\rangle$, i.e., the transformed (primed) states have the same symmetry as the original states.

Figure 12 shows the KH and the velocity gauge probability density for the excursion amplitude $\hat{\alpha} = 10$. The target energy was $\mathcal{E} = -0.08$ where in Fig. 9 the almost degenerate ground and first excited state energies for $\hat{\alpha} = 10$ are. The KH probability density fits to the KH potential

$$V_{\rm KH}(x) = \frac{1}{2\pi}\int_0^{2\pi} V[x + \hat{\alpha}\sin\tau]\,{\rm d}\tau, \tag{122}$$

shown in the lower panel. The actual calculation was performed for $\omega_1 = 4$ and a trapezoidal (10,1180,10)-pulse. The target energy $\mathcal{E}$ in (110) is scanned through the energy region of interest, and the Floquet energy is hit when the value of the integral is maximum. If one uses the same integration time for different $\mathcal{E}$ the integral

$$N_\mathcal{E} = \int_{-\infty}^{\infty} |\zeta_\mathcal{E}(x)|^2\,{\rm d}x \tag{123}$$

is a measure for the population of the Floquet state in the actual pulse.

The Floquet energies are invariant under the transformations $\hat{G}(t)$ while both the Floquet states $|\zeta_{\beta n}\rangle$ and their populations are not. In particular, in the high-frequency limit one expects that only the eigenstates in the KH potential (122) matter [47]. These states correspond to the Floquet energies in the Floquet block $n = 0$. Hence, the energy spectrum in the KH frame is expected to be much more localized around $n = 0$ than in velocity gauge. This is confirmed by Fig. 13. Instead of using the even or odd test functions in (108) and spatial integration we analyzed the wave function $\Psi(x,t)$ at $x_{\rm test} = 2$, i.e., we calculated

$$Q'(\mathcal{E}) = \sum_{\beta n}\int_{t_1}^{t_2} {\rm e}^{-{\rm i}t(\epsilon_\beta + n\omega_1 - \mathcal{E})}{\rm d}t\;\zeta_{\beta n}(x_{\rm test}). \tag{124}$$

This avoids the transformation of the entire wave function to the KH frame and yields similar results as long as one chooses $x_{\rm test}$ in a region where the wave function is sizeable and both odd and even parity wave

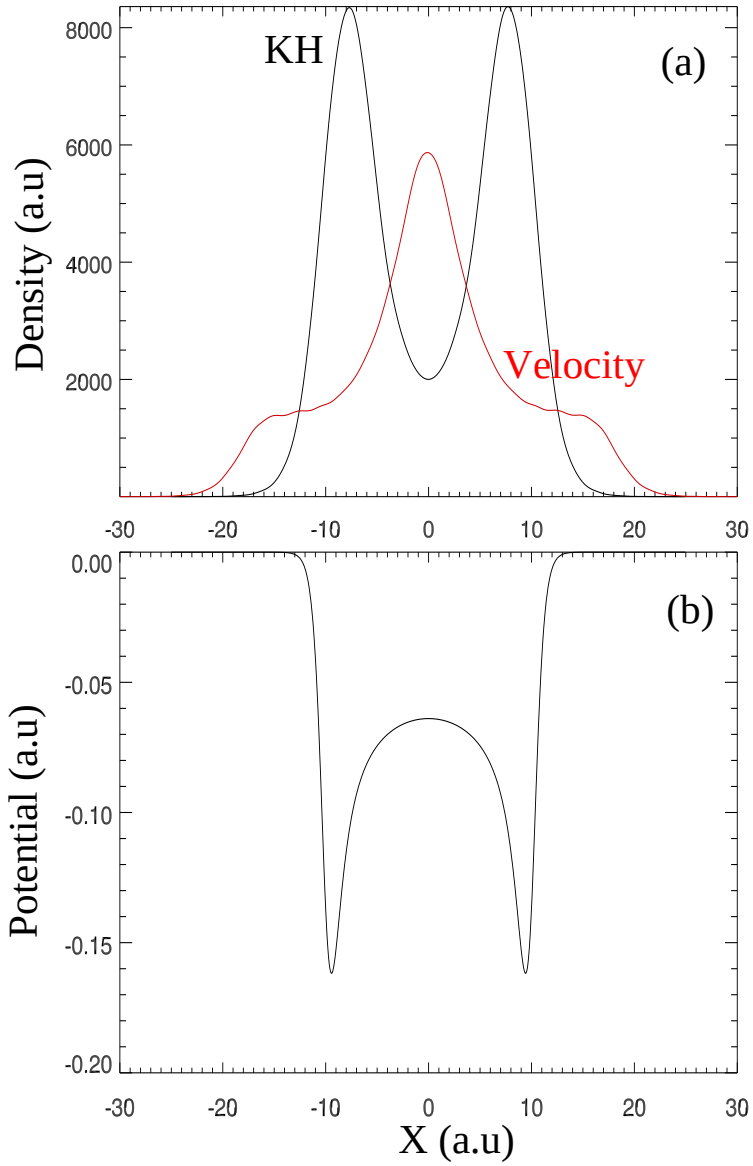

Figure 12: (a) KH and the velocity gauge probability density for the excursion amplitude $\hat{\alpha} = 10$ and target energy $\mathcal{E} = -0.08$. (b) KH potential [48].

functions contribute (for $x_{\text{test}} = 0$ only contributions from even Floquet states would be visible). Figure 13 shows that the populations of Floquet states in different frames (or gauges) are different while the Floquet energies are the same. Of course, the gauge- or frame-dependence should vanish when field-free observables, such as photo-electron spectra are considered.

4.4 photo-electron spectra

Without laser field the continuum states of the Pöschl-Teller potential have energies $\mathcal{E} > 0$. With laser field all continuum states are contained in each Floquet block so that overlaps of the continua of all blocks with dressed bound states of all blocks are possible. However, we expect the dressed bound states of the $n = 0$ block to dominate since they are the main ones being populated during the switching-on of the laser. Let us first discuss the case where $\omega_1 > \min \epsilon_\beta$, i.e., a single photon is sufficient for ionization. Then the dressed bound state in Floquet block n with energy $\epsilon_\beta + n\omega_1$ overlaps with continuum states of all the Floquet blocks $m < n$. In particular, $\epsilon_\beta + n\omega_1$ overlaps with the continuum state of energy ϵ_p of the zeroth Floquet block, where p indicates the asymptotic momentum of this continuum state.

We will now turn to the question of how the manifold of mixtures of bound and continuum Floquet states converts to an observable photo-electron spectrum when the pulse is switched off. Figure 14 shows a time-resolved Floquet spectra in velocity gauge for a 100-cycle $\sin^2$-pulse of excursion amplitude, $\hat{\alpha} = 10$ and frequency, $\omega_1 = 4$ for $x_{\text{test}} = 2$ (i.e., "inside" the potential) and a time-window of width $t_{\text{w}} = t_2 - t_1 = 50$ in (124). The time on the horizontal axis is t_1 so that the spectra for times $t_1 > 100T = 157.1$ (indicated by the vertical black line) were obtained from field-free states, i.e.,

$$\begin{aligned} Q^{(0)}(\mathcal{E}, t_1) &= \int_{t_1}^{t_1+t_{\text{w}}} \mathrm{e}^{\mathrm{i}\mathcal{E}t} \Psi(x_0, t)\, \mathrm{d}t \\ &= \sum_\beta \zeta_\beta^{(0)}(x_0) \int_{t_1}^{t_1+t_{\text{w}}} \mathrm{e}^{-\mathrm{i}t(\epsilon_\beta^{(0)} - \mathcal{E})} \mathrm{d}t. \end{aligned} \tag{125}$$

Figure 14a shows that while the pulse is on the bound state population is distributed over many Floquet blocks. As the pulse is switched off, all the Floquet populations for $n \neq 0$ disappear, and only the ground state

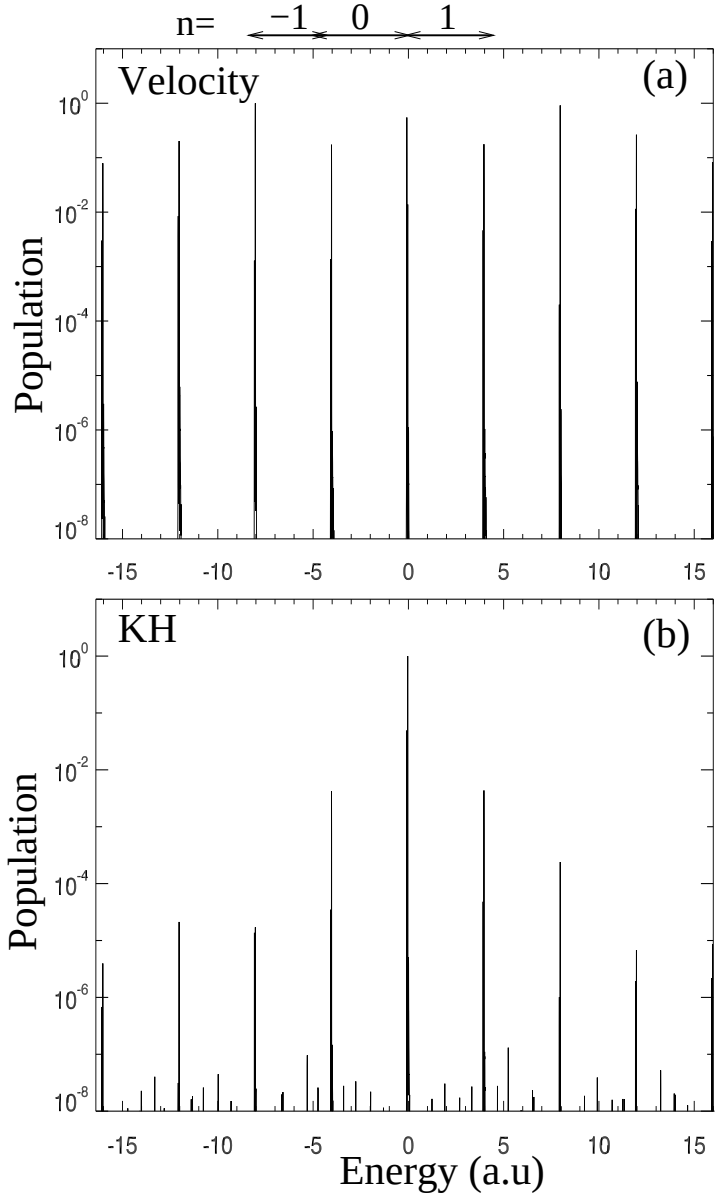

Figure 13: Floquet spectra for $\hat{\alpha} = 10$, $\omega_1 = 4$, and a (10,1180,10)-pulse in (a) velocity gauge (with the $A^2(t)/2$-term transformed away) and (b) in the KH frame. In the KH frame mainly the $n = 0$-Floquet block counts [48].

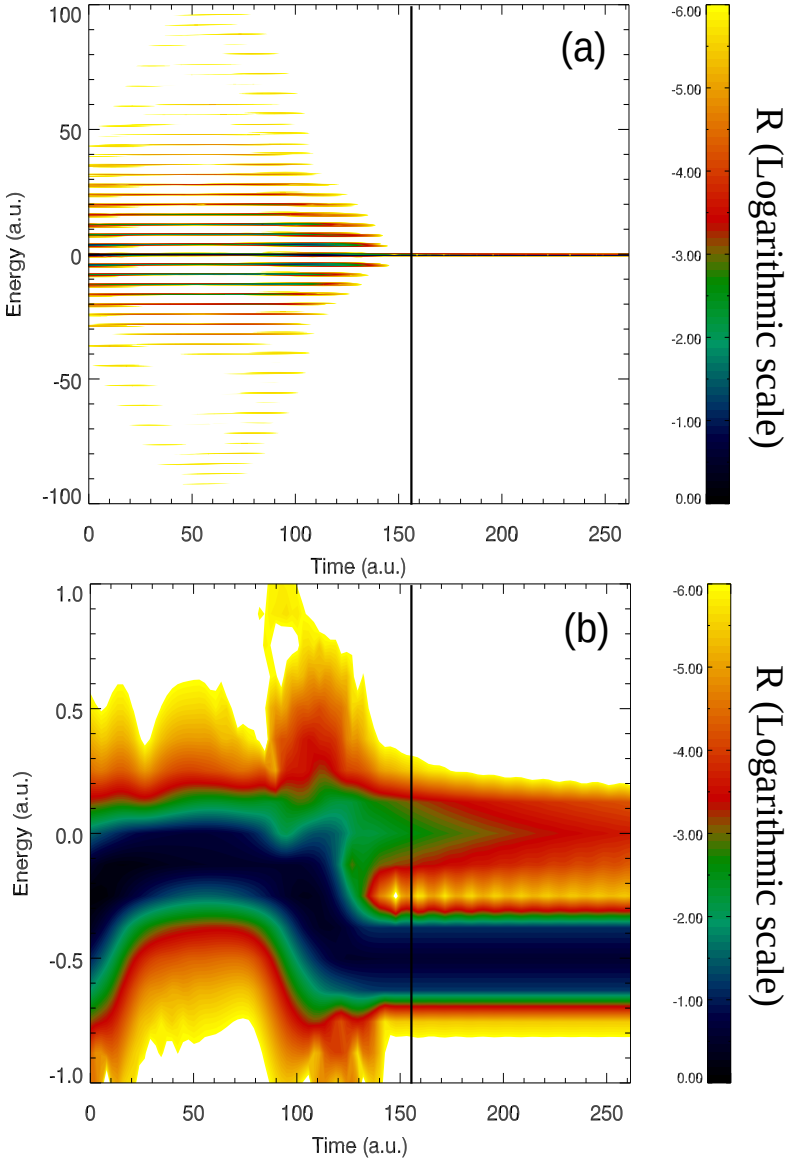

Figure 14: Time-resolved Floquet spectra for a 100-cycle $\sin^2$-pulse of amplitude $\hat{\alpha} = 10$, $\omega_1 = 4$, $x_{\text{test}} = 2$ (i.e., "inside" the potential), and a time-window of width $t_w = t_2 - t_1 = 50$. The vertical line indicates the end of the pulse. Panel (b) is a close-up of the energy region around $\epsilon_0^{(0)} = -0.5$ in (a). The calculation was performed in velocity gauge (with the $A^2(t)/2$-term transformed away) [48].

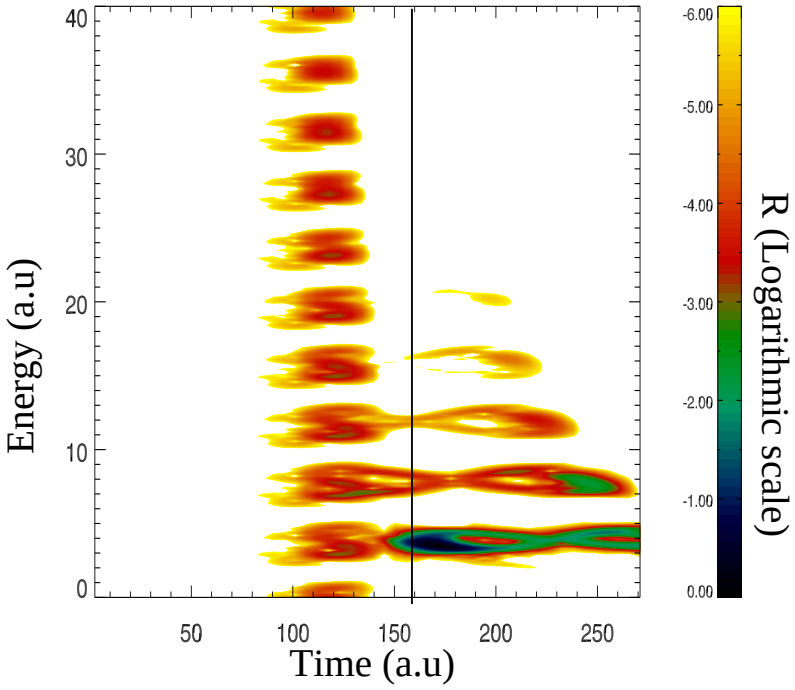

Figure 15: Same as in Fig. 14 but for $x_{\text{test}} = 471.3$ [48].

population inside the potential with energy $\epsilon_0^{(0)}$ remains. This is because we analyzed the spectrum at the position $x_{\text{test}} = 2$. Contributions to the wave function corresponding to electrons in the continuum, traveling with an asymptotic momentum p quickly decay at $x_{\text{test}} = 2$. Figure 14b shows a close-up of the region around $\epsilon_0^{(0)}$. With increasing envelope of the laser pulse the dominant Floquet population shifts adiabatically from the field-free value $\epsilon_0^{(0)} = -0.5$ to the ground state energy of the KH potential $\epsilon_0^{(\text{KH})} \simeq -0.09$ (see Fig. 9 for $\hat{\alpha} = 10$) and back. Note that although the calculation was performed in velocity gauge the KH ground state energy shows up here because the Floquet quasi-energies are frame- and gauge-independent.

Figure 15 shows the same analysis for $x_{\text{test}} = 471.3$, i.e., "far away" from the atom so that it takes some time until probability density arrives at all around $t = 100$. It is interesting to observe that in velocity gauge (with the $A^2(t)/2$-term transformed-away) this "arrival time" during the pulse is independent of the energy. As the laser pulse is switched off at $t = 157.1$ many Floquet channels close. However, because electrons

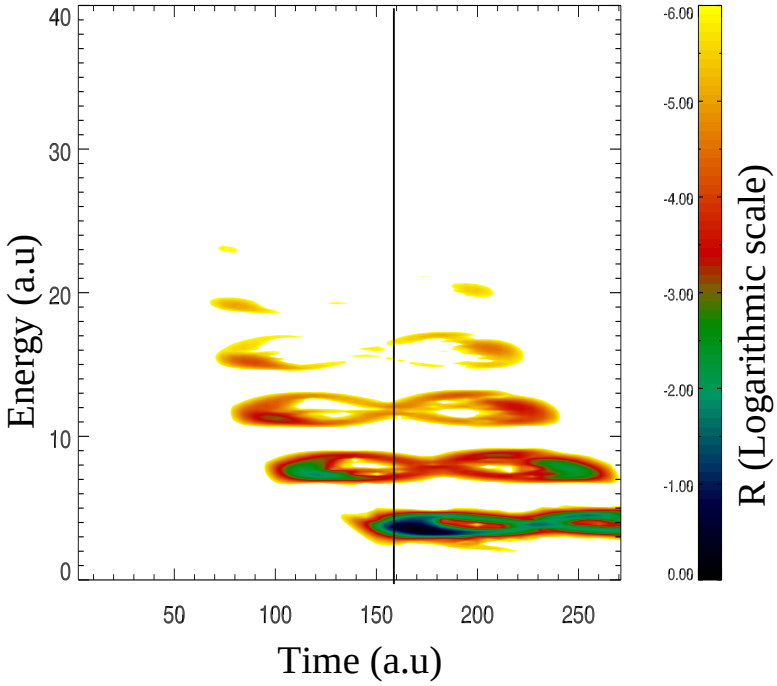

Figure 16: Same as Fig. 15 but for the KH frame [48].

are still on their way from the atom to the "virtual detector" at $x_{\text{test}} = 471.3$ we are able to "measure" the field-free photo-electron spectrum of the electrons emitted in that direction. The time these free electrons need to pass the virtual detector decreases with increasing energy, as is seen in Fig. 15 where the width of the traces for $t > 157.1$ decrease with increasing energy. The five traces visible are separated by ω_1 and correspond to ATI peaks [55]. They are quite broad in energy because of the change of the ionization potential (from field-free value to KH value and back). Their figure-eight shape in the contour plot of Fig. 15 is a peculiarity of the $\sin^2$-pulse shape.

Figure 16 shows the corresponding result obtained for the KH frame. We see that in the KH frame only those states are populated in the laser field which actually contribute to the final field-free spectrum. This is because the KH potential at $x_{\text{test}} = 471.3$ is almost identical to the field-free one so that outgoing electrons are not affected anymore by the oscillating KH binding potential. It is also seen in Fig. 16 that the most energetic electrons arrive earlier at x_{test} unlike the velocity gauge-result in Fig. 15.

4.5 CHANNEL-CLOSINGS

So far we studied mainly high-frequency phenomena where the Floquet blocks are well separated. However, there are plenty of interesting, non-perturbative phenomena occurring at low frequencies where the pondermotive energy $U_p = \hat{E}^2/4\omega_1^2$ can be large at nowadays available laser intensities $\hat{E}^2$. Examples are tunneling ionization and high-order ATI due to rescattering of electrons [56, 57]. In this Section we choose so-called "channel-closing" (see [58] and references therein) as a low-frequency phenomenon to illustrate our method.

The TDSE was solved for a trapezoidal pulse of frequency $\omega_1 = 0.08$. On the energy scale of the ionization potential the Floquet blocks are packed much closer in this case, meaning that many photons are necessary for ionization. In Fig. 17 we plot the Floquet energy spectrum R in a certain range of excursion amplitude $\hat{\alpha} = \hat{E}/\omega_1^2$ and energy $\mathcal{E}$ around the field-free continuum threshold (other relevant parameters given in the figure caption). The calculation was performed in velocity gauge (with the $A^2(t)/2$-term transformed-away) using again the potential (105). There is a clear down-shift of all the populated Floquet levels with increasing laser amplitude. This AC Stark shift is also referred to as the "pondermotive shift" because the effective ionization potential is increased by U_p (see Chapter 1). In fact, the energy in the photo-electron spectrum is given by

$$\mathcal{E} = \frac{p^2}{2} = n\hbar\omega_1 - (|\mathcal{E}_0| + U_p), \tag{126}$$

(provided the AC Stark shift of the initial state is negligible, which at long wavelengths often is the case). $\mathcal{E}_i$ is the initial electron energy and n is the number of photons absorbed. In order to reach the continuum at all $n > (|\mathcal{E}_0| + U_p)/\hbar\omega_1$ photons have to be absorbed. As the intensity, and thus U_p, is increased, more and more photons are needed for ionization. When n photons are no longer sufficient but $n+1$ photons are needed the n-photon channel closing occurs. In the contour plot shown in Fig. 17 a channel closing manifests itself as a crossing of a Floquet quasi-energy and the continuum threshold. Now, the interesting feature in Fig. 17 is the zero-energy LIS. Such LIS were also observed in Ref. [59], where also their connection with experimentally observed enhancements in the photo-electron spectra at high energies [60] was established. The parity of both states involved in the crossing in Fig. 17 is

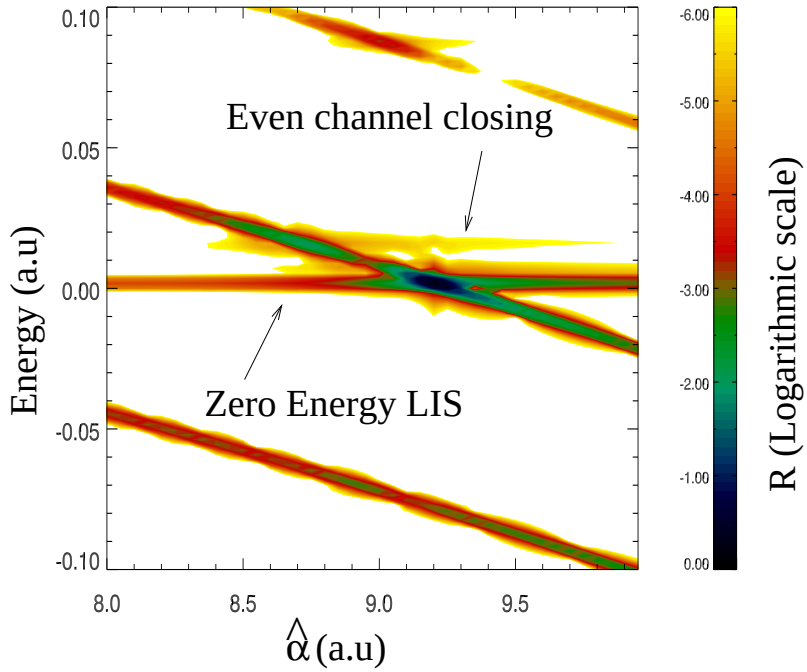

Figure 17: Logarithmic plot of $R = |Q_+|^2 + |Q_-|^2$ vs $\mathcal{E}$ and $\hat{\alpha}$, showing the (populated) field-dressed states for $\omega_1 = 0.08$ and a trapezoidal (4,40,4)-pulse [48].

even, and it is known that depending on the parity of the states, channel closings affect the photo-electron spectrum differently [59, 61].

In our model, for the first even channel closing eight photons are needed. It occurs at $\hat{\alpha} = 9.354$. One would expect that channel closings only affect low-energy electrons because the kinetic energy of the electrons whose channel is about to close is low. Hence, as the intensity is increased the yield of ATI peaks at energies, say, $> 5U_p$ should increase monotonously as well. However, near even photon channel closing there is a marked increase in the photo-electron yield [58, 59, 61]. Instead, when in odd photon channel closings the odd-parity LIS crosses the zero-energy LIS, such enhancements are absent. The first odd photon channel closing occurs around $\hat{\alpha} = 11.55$, the next even photon channel closing occurs around $\hat{\alpha} = 13.55$. The photo-electron spectra obtained using our Floquet method confirm the presence and absence of enhancements at even and odd channel closings, respectively, as shown in Fig 18.

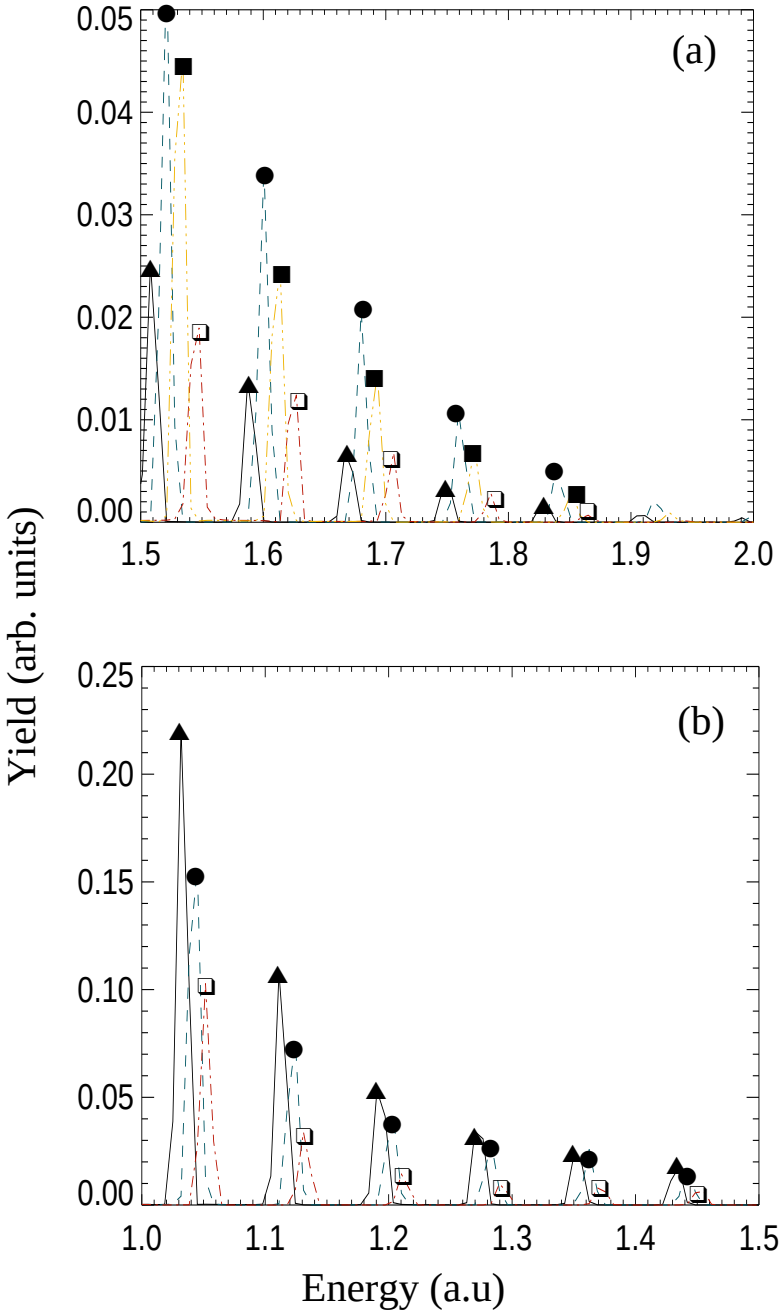

Figure 18: (a) photo-electron spectra for energies around $5U_p$, $U_p = 0.3$. Non-monotonic behavior of yield with existence of a maxima at channel closing intensity for even photon channel closing. Transparent square: 13.0, solid square: 13.3, circles: 13.55, triangles: 13.8. (b) Same for an odd channel closing, $U_p = 0.21$, where a monotonic behavior of the yield with increasing intensity is observed. Triangles: $\alpha = 11.8$, circles: $\alpha = 11.55$, transparent squares: $\alpha = 11.3$ [48].

The method 4.2 is straightforwardly extendable to three dimensions (see appendix C). We think the method is most useful for researchers running codes to solve the time-dependent Schrödinger equation in real time. By saving the wave function at selected spatial positions as a function of time during the interaction with the laser field the analysis in terms of light-induced states can be easily performed *a posteriori*. The method appears to be most adequate at high frequencies where the Floquet blocks are clearly separated. Its application to correlated multi-electron systems may be very fruitful, as the understanding of field-dressed, multiply-excited or autoionizing states is still poor.

5

FLOQUET THEORY AND TIME-DEPENDENT DENSITY FUNCTIONAL THEORY

Since a Floquet analysis of real time wave functions offers an insight into the physical nature of the phenomena it is tempting to incorporate the analysis in TDDFT, as portrayed in Sec. 3.3.6. If this could be done then the solution of N one-particle time-dependent equations would reduce to the solution of N one-particle time-independent equations. This would simplify periodic time-dependent many-body problems significantly. Already at the beginning of the application of density-functional theory to time-dependent systems attempts were made to incorporate Floquet theory in a density-functional framework [62, 63]. A minimization principle was proposed, which was perturbative in nature and hence valid only for weak and off-resonant fields. However, even if these conditions are met there are problems with defining a proper adiabatic limit, which is fundamental to the proposed minimization procedure [64]. The problems arise due to the fact that Floquet theory maps the quasi-spectrum of the time-dependent problem into an interval of length ω, i.e., the frequency of the periodicity employed. In any interval $I = \{x - \omega/2, x + \omega/2\}$ for $x \in \mathbb{R}$ arbitrary we find infinitely many quasi-eigenenergies (they are dense in I) and thus infinitely many eigenfunctions around every point in the quasi-spectrum. A consequence of this is that there is no unique final state to which the system tends as the external perturbation is turned off adiabatically. In order to restore the adiabatic limit a truncation to a finite basis is usually employed, which is anyway unavoidable in practical calculations.

In Refs. [4,46,65,66] Floquet-DFT approaches were pursued for non perturbative fields and later criticized in Refs. [67,68] where the authors also suggested to embark upon the problem from a TDDFT point of view, thereby avoiding the minimization problem. The basic question then remains whether a Floquet basis can be found for the associated KS system, i.e., whether the KS Hamiltonian itself is periodic. Known explicit expressions for the exchange-correlation potential in the time-dependent KS Hamiltonian such as the adiabatic local density approximation or

generalized gradient approximations [6, 7] have the feature that a periodic density will lead to a periodic KS Hamiltonian (with the same period) since the adiabatic Hxc potentials depend on the instantaneous density only. However, the density does not have to be periodic and, in fact, it generally is not, as we have demonstrated in [44] and shall explain in this work. On the other hand, even if an approximate functional leads to an aperiodic KS potential because of, e.g., an aperiodic density, this does not yet demonstrate the incompatibility of TDDFT and Floquet theory, because the unknown *exact* KS potential nevertheless could be periodic. We will show by means of numerical and analytical counter examples that this, unfortunately, is not the case and thus TDDFT is, in general, not compatible with Floquet theory [44].

The content of this chapter has been published in [44].

5.1 periodic or aperiodic kohn-sham hamiltonian?

In order to prove that Floquet theory is generally not applicable to TDDFT it certainly is sufficient to find one counterexample. However, a Floquet approach might still be useful as an approximative approach, especially given the fact that TDDFT in practice is itself approximative anyway. Hence, we analyze under which circumstances the KS Hamiltonian is periodic or not. The initial TDSE state of the model Helium is chosen to be the spin-singlet ground state of the interacting system 22.

As seen in the previous Chapter, by controlling the laser parameters we can either have an adiabatic evolution of the field-free state $\Psi_0(x_1, x_2)$ to a single, field-dressed (Floquet) state or a non-adiabatic one, where several Floquet states are populated. The laser intensity, frequency and the ramping time decide on the adiabaticity of the time-evolution of the interacting system. For adiabatic evolution we have in the TDSE-Floquet calculation only one relevant Floquet-state index α in the TDSE analog of (100),

$$\Psi(x, y, t) = \sum_{\alpha} c_{\alpha} \mathrm{e}^{-\mathrm{i}\tilde{\varsigma}_{\alpha} t} \sum_{l} \mathrm{e}^{-\mathrm{i}l\omega_1 t} \varphi_{\alpha,l}(x, y). \tag{127}$$

Hence, in this case

$$\Psi(x, y, t) \sim \mathrm{e}^{-\mathrm{i}\tilde{\varsigma}_{\alpha} t} \sum_{l} \mathrm{e}^{-\mathrm{i}l\omega_1 t} \varphi_{\alpha,l}(x, y), \tag{128}$$

and the density $n(x,t) = 2\int \mathrm{d}x' \, |\Psi(x,x',t)|^2$ will only have frequency components proportional to multiples of the laser frequency ω_1. The KS Hamiltonian depends on the density. If the KS potential is periodic with respect to integer multiples of the laser frequency there would be no problem because $\hat{H}_{\mathrm{KS}}([n(t+T)];t+T) = \hat{H}_{\mathrm{KS}}([n(t)];t)$, and thus the Floquet theorem still holds. Instead, fractional harmonics or, even worse, incommensurate frequencies in $\hat{H}_{\mathrm{KS}}([n(t)];t)$ would render the Floquet theorem inapplicable. If more than one Floquet state is populated, say $\alpha = \alpha_1$ and α_2, the Fourier-transformed density $n(x,\omega)$ will also have frequency components proportional to the quasi energy difference $|\xi_{\alpha_2} - \xi_{\alpha_1}|$. It would be astonishing if the unknown *exact* $v_{\mathrm{xc}}([n];x)$ was able to remove such frequencies from $\hat{H}_{\mathrm{KS}}([n(t)];t)$. However, in order to *prove* that in general the exact $v_{\mathrm{xc}}([n];x)$ contains frequency components different from ω_1 we construct the exact $v_{\mathrm{xc}}([n];x)$ explicitly in the following for both the adiabatic as well as the non-adiabatic evolution of the field-free state to the field-dressed states.

From the exact solution of the TDSE corresponding to the Hamiltonian (17) for our model Helium atom, we can compute the exact KS potential via the technique outlined in Sec. 3.3.5. Once the exact KS potential is computed, it is Fourier-transformed in time to investigate its periodicity.

Besides the basic problem of the periodicity of the KS potential for a given interacting density, there is the inherent non-linearity of the KS scheme. Even though the exact KS potential might be periodic for a certain problem, it is far from obvious that one can employ a Floquet-based KS scheme to predict it. For instance, although an adiabatic approximation, e.g., in the two-electron spin-singlet case the exact exchange-only approximation $v_{\mathrm{Hx}}^{(\mathrm{exact})}([n];x) = \int \mathrm{d}x' \, [n(x',t)/2]/\sqrt{(x-x')^2+\epsilon}$, does inherit the periodicity of the density, it is not guaranteed that the non-linear KS equations produce a periodic $n(x,t)$. This becomes obvious when we consider the iterative solution of the KS equations, where we start with an initial guess for the density that is periodic with ω_1. We then have a periodic KS Hamiltonian from which we can (since in every iterative step we have a linear partial differential equation) infer a Floquet basis. We then solve the resulting linear equations and obtain a new density. This density will in general not be periodic and we no longer find a Floquet basis with period ω_1 only. This makes the problem of the non-linearity in connection with a Floquet approach evident.

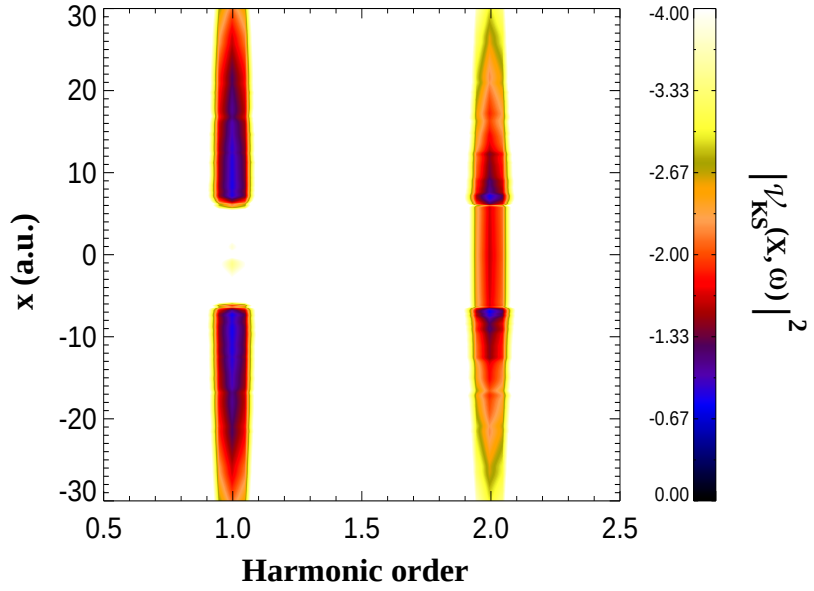

Figure 19: Logarithmic plot of $|v_{\mathrm{KS}}(x,\omega)|^2$ [from its rescaled maximum value 10^0 (black) "down to" 10^{-4} (white)] for $\omega_1 = 0.056$, $\hat{E} = 0.063$, two-cycle ramp-up, and 16 cycles constant amplitude. Notice that only harmonics of the laser frequency are present over a dynamic range of four orders of magnitude. Superpositions of Floquet states do not play a role, the dynamics are sufficiently adiabatic, the Floquet theorem is applicable to $\hat{H}_{\mathrm{KS}}([n(t)];t)$ [44].

5.1.1 *Adiabatic and periodic example*

First we consider an 800-nm ($\omega_1 = 0.056$) laser pulse with two cycles ramp-up and 16 cycles of constant amplitude. The electric field amplitude is $\hat{E} = 0.063$, corresponding to a laser intensity of 1.4×10^{14} W/cm^2. It turns out that in this case the density dynamics are periodic with the laser period. In Fig. 19 we plot the exact $|v_{\mathrm{KS}}(x,\omega)|^2$ over four orders of magnitude vs the harmonic order ω/ω_1. Only harmonics of the laser frequency at all space points of the KS potential are visible. An analysis as proposed in [48] and Sec. 4.2 reveals that only a single Floquet-state of the interacting system is populated, showing that the dynamics are adiabatic. The Floquet theorem is applicable to the KS system in this case, as $\hat{H}_{\mathrm{KS}}([n(t+T)];t+T) = \hat{H}_{\mathrm{KS}}([n(t)];t)$ to a high degree of accuracy.

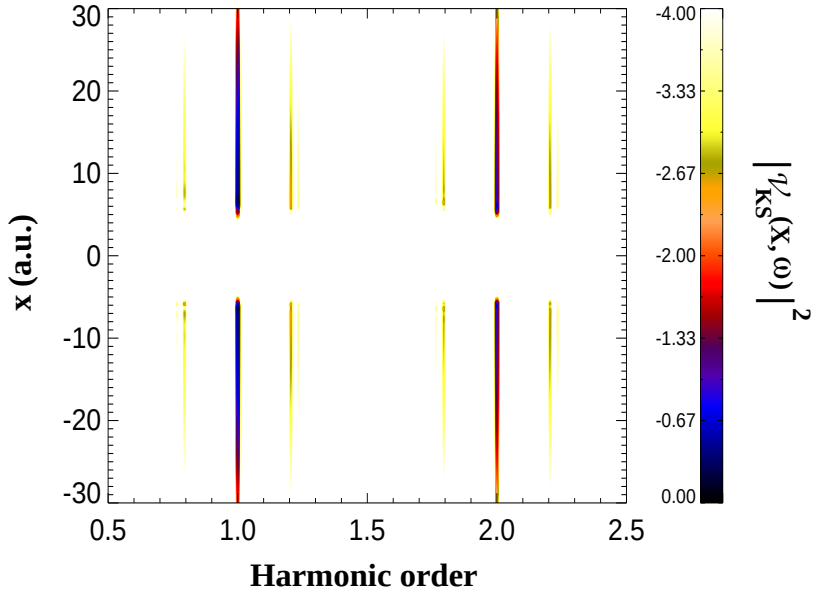

Figure 20: As Fig. 19 but for $\omega_1 = 2.6$, $\hat{E} = 0.34$, four-cycle ramp-up, and 172 cycles constant amplitude. The Fourier-transformed potential displays anharmonic frequency components, i.e., it is aperiodic [44].

5.1.2 *Non-adiabatic and aperiodic example*

As a second example we chose a short-wavelength 17.5-nm ($\omega_1 = 2.6$) laser pulse with four cycles ramp-up and 172 cycles of constant amplitude. The electric field amplitude $\hat{E} = 0.34$ corresponds to a laser intensity of 4×10^{15} W/cm^2. The fast ramping induces a non-adiabatic time-evolution and results in a superposition of Floquet states in the TDSE result. The exact KS potential oscillates with periods related to the inverse of the quasi energy differences. In Fig. 20, this new timescale manifests itself as side bands around the multiples of the laser frequency. The quasi energy differences are determined by the field-free spectrum of the system under study and by the AC Stark shifts so that it may well happen that they are irrational fractions or multiples of ω_1. In that case even a $T' > T = 2\pi/\omega_1$ for which $\hat{H}_{\mathrm{KS}}(t + T') = \hat{H}_{\mathrm{KS}}(t)$ does not exist.

5.1.3 *Resonant interaction*

When the laser is tuned to the exact resonance between the initial (ground) state and a dipole-accessible excited state, Rabi-oscillations set in, typically on a time scale that is much longer than the laser period so that for the Rabi frequency Ω one has $\Omega \ll \omega_1$. In this case the density is periodic with the Rabi-frequency Ω, not with the laser frequency ω_1. At time $T_{1/2} = \pi/\Omega$ the upper state is populated, at time $2\pi/\Omega$ the initial state is populated again. The Rabi-frequency depends on the electric field amplitude $\hat{E}$ of the laser and the transition dipole matrix element μ_{01} between the two bound states involved. Rabi-oscillations are not captured in TDDFT when known and practicable adiabatic exchange-correlation potentials are used. Of course, the density dynamics between the two states are correctly described when the exact KS potential is used, for instance for the numerically exactly solvable model-He system employed in this work. It is known that after the time $T_{1/2}$, when the single-particle density $n(x, T_{1/2})$ is that of the *excited interacting system*, the exact KS potential is the *ground state potential* to that density [14, 15]. In fact, there is no stationary state in the KS potential to which the population may be transferred. Hence, the exact KS system governs the dynamics by an "adiabatic deformation" of the ground state density. Despite this extremely simple "Rabi-flopping" dynamics, resonant interactions are among the worst cases for TDDFT with known and practicable exchange-correlation potentials.

It is well known that a Floquet treatment of the TDSE leads to avoided crossings of the two field-dressed state energies when plotted as a function of laser frequency [3] (see also Sec. 4.2) . At exact resonance the two Floquet states are equally populated and separated in energy by $\hbar\Omega$. Hence, resonant interaction is a prime example where a superposition of Floquet states plays a role even if the laser pulse was turned on adiabatically.

The laser frequency in our model simulation was tuned to be at resonance between the ground spin-singlet state and the first excited spin-singlet state of the model Helium atom, $\omega = \mathcal{E}_1 - \mathcal{E}_0 = 0.533$ [14]. For the chosen field amplitude $\hat{E} = 0.016$ (corresponding to a laser intensity of 9×10^{12} W/cm^2) the ground state population reaches zero at $T_{1/2} \approx 174$, i.e., $\Omega = 0.018$. Figure 21 shows $|v_{\mathrm{KS}}(x, \omega)|^2$ for two cycles ramp-up and 148 cycles of constant amplitude. The Fourier-transformed

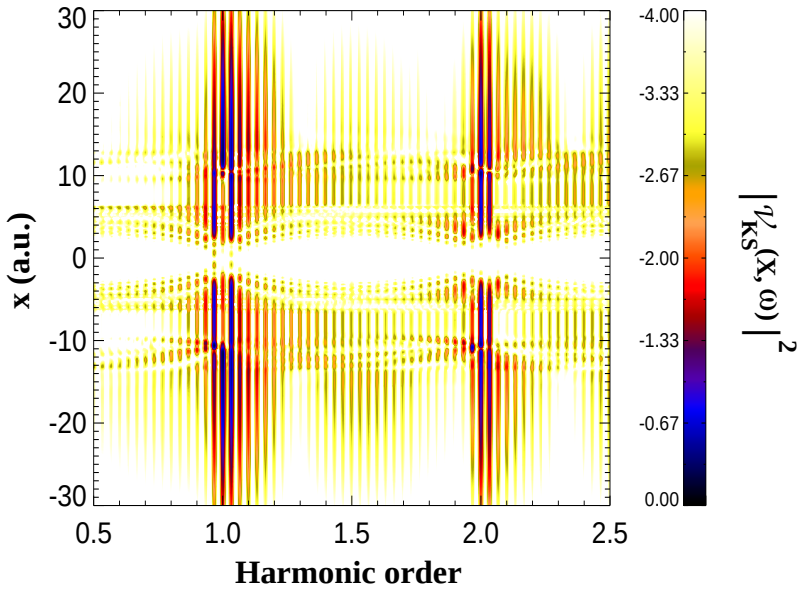

Figure 21: As Fig. 19 but for the resonant interaction with $\omega = \mathcal{E}_1 - \mathcal{E}_0 = 0.533$, $\hat{E} = 0.016$, two cycles ramp-up, and 148 cycles constant amplitude. Peaks at positions $q\omega_1 \pm p\Omega$ with $q, p \in \mathbb{Z}$ are seen [44].

potential shows strong sideband peaks at $q\omega_1 \pm p\Omega$ with $q, p \in \mathbb{Z}$. Hence, while in the previous example of non-adiabatic ramping one might argue that the anharmonic peaks in the spectra are weak and therefore could be ignored, a resonant interaction generates sideband peaks of strengths comparable to the harmonics.

5.2 INITIAL STATE CHOICE

For the above examples of non-adiabatic ramping or resonant interaction a minimization procedure with a finite Floquet basis would lead to a laser-aperiodic KS Hamiltonian that renders the Floquet theorem inapplicable in the first place. From the TDDFT perspective we obtain a laser-aperiodic KS Hamiltonian because of the time evolution starting from the chosen initial state. However, in TDDFT $\hat{H}_{\mathrm{KS}}([n(t)];t)$ should actually read $\hat{H}_{\mathrm{KS}}([n(t),\Psi_0,\{\Phi_{0k}\}];t)$ because of the dependence of the time-dependent KS potential on both the interacting initial state Ψ_0 and the KS initial states Φ_{0k} [7,62]. Thus a loophole for a most stubborn assumable proponent of TDDFT-Floquet theory remains: a different choice

of initial KS states $\Phi_{0k}(x) = \Phi_k(x, t = 0)$ could keep the KS Hamiltonian periodic in T. In this Section we give a counter example for which *all* possible initial states lead to laser-aperiodic KS potentials if the density is laser-aperiodic. To do so analytically we construct a KS system of two non-interacting electrons on a quantum ring of diameter L so that we have periodic boundary conditions [41]. This makes it an ideal system to analyze the time-periodicity of the KS Hamiltonian for the various possible initial states. For spin-singlet states of these electrons one can describe the system by a single KS orbital (88) as in our model Helium system above (in the limit $L \to \infty$ the quantum ring becomes equivalent to the Helium model [1]). Following the procedure outlined in Sec. 3.3.5 the potential can be written in terms of the density and the phase of the KS orbital as

$$\begin{aligned} & v_{\mathrm{KS}}([m,n],x,t) \\ &= \frac{1}{2}\frac{\partial_x^2\sqrt{n(x,t)}}{\sqrt{n(x,t)}} - \partial_t S([m,n],x,t) - \frac{1}{2}[\partial_x S([m,n],x,t)]^2, \end{aligned} \tag{129}$$

which is an explicit functional of the density $n = n(x,t)$ and an integer number $m \in \mathbb{Z}$. As shown in Ref. [41], for periodic boundary conditions the phase S can be written in the integral form

$$\begin{aligned} S([m,n],x,t) &= \int_0^L dy\, K_t(x,y)\partial_t n(y,t) \\ &+ \frac{2\pi m}{\int_0^L \frac{dz}{n(z,t)}}\int_0^x \frac{dz}{n(z,t)}, \end{aligned} \tag{130}$$

where the Green's function, $K_t(x,y)$ is defined as

$$\begin{aligned} K_t(x,y) &= \frac{1}{2}[\theta(y-x) - \theta(x-y)]\int_x^y \frac{dz}{n(z,t)} \\ &- \frac{\eta(x,t)\eta(y,t)}{\int_0^L \frac{dz}{n(z,t)}}, \end{aligned} \tag{131}$$

with θ the Heaviside step function and

$$\eta(x,t) = \frac{1}{2}\left(\int_0^x \frac{dy}{n(y,t)} + \int_L^x \frac{dy}{n(y,t)}\right). \tag{132}$$

[1] Note that in the case $L \to \infty$ only one square-integrable solution to (89) exists and thus we do not have different initial states (numbered by $m \in \mathbb{Z}$) for a given density in time. In order to investigate the initial-state dependence we therefore consider periodic potentials only.

Since the KS orbital obeys the periodic boundary conditions, the phase S has to satisfy

$$S(L,t) = S(0,t) + 2\pi m \tag{133}$$
$$\partial_x S(L,t) = \partial_x S(0,t). \tag{134}$$

Hence the integer m plays the role of labeling all the possible KS orbitals (for different initial-state choices) that are consistent with the density $n(x,t)$.

If we assume that

$$n(x,t+T) = n(x,t), \tag{135}$$

we have

$$\int_x^y \frac{dz}{n(z,t)} = \int_x^y \frac{dz}{n(z,t+T)}. \tag{136}$$

Since $K_t(x,y)$ in Eq. (131) consists only of such time-periodic integrals

$$K_t(x,y) = K_{t+T}(x,y). \tag{137}$$

Also, since

$$\partial_t n(x,t)|_t = \partial_t n(x,t)|_{t+T}, \tag{138}$$

we conclude from (130) that

$$S([m,n],x,t) = S([m,n],x,t+T). \tag{139}$$

The first term on the right hand side of Eq. (129) is also periodic with the same period as the density. This implies that the entire potential is periodic with the same period as the density, i.e.,

$$v_{\mathrm{KS}}([m,n],x,t) = v_{\mathrm{KS}}([m,n],x,t+T). \tag{140}$$

Hence for any possible initial state (labeled by the index m) and a density periodic with the period of the external field we find that the KS Hamiltonian is also periodic with the period of the external field.

For the Floquet theorem to be applicable in a TDDFT framework, the time-dependent KS Hamiltonian must be periodic with the period of the external field $T = 2\pi/\omega_1$ only, i.e.,

$$v_{\mathrm{KS}}([m,n],x,t) = v_{\mathrm{KS}}([m,n],x,t+T). \tag{141}$$

Consider now the density being periodic with a period T' different from the period of the external field,

$$n(x,t) = n(x,t+T'), \tag{142}$$

as in the above examples in Secs. 5.1.2 and 5.1.3. The periods T and T' are incommensurate in general. We just have proven that the KS potential is periodic with the same period as the density, which implies that

$$v_{\mathrm{KS}}([m,n],x,t) = v_{\mathrm{KS}}([m,n],x,t+T'). \tag{143}$$

This is in contradiction with the assumption of only one period $T = 2\pi/\omega_1$ of Eq. (141) which allows the Floquet theorem to be applied in the first place. Hence, the Floquet theorem cannot be applied.

Here, for our example for which we are able to write down an explicit expression for the KS potential, we have proven that for *any* initial KS state it is impossible to have a laser-periodic KS potential when the density has another period.

From these results we conclude that the Floquet theorem is in general inapplicable to TDDFT for intense and resonant laser fields.

6

AUTOIONIZATION IN TIME-DEPENDENT DENSITY FUNCTIONAL THEORY

In this Chapter we compute the exact KS potential for the highly correlated process of autoionization [69]. Exact studies such as this have led to development of better exchange-correlation potentials in TDDFT for quite a few correlated processes [13, 39]. As enumerated in the table in section 3.3.5 we find that such studies often reveal the essential features that any exchange-correlation potential should possess to be able to describe a correlated process correctly. Since autoionization occurs only due to electron-electron interaction the process is correlated. Autoionization in a Helium-like system results in the emission of an electron while the second electron remains bound in an ionic state. We consider again our model Helium atom to study the process.

Let the energy of the autoionizing state be $\mathcal{E}_{\mathrm{AI}}$. The kinetic energy of the emitted electron $\frac{k^2}{2}$ is dictated by the energy conservation,

$$\mathcal{E}_{\mathrm{AI}} = \mathcal{E}_{\mathrm{He}^+} + \frac{k^2}{2}. \tag{144}$$

The ionic bound state with energy $\mathcal{E}_{\mathrm{He}^+}$ can be either the ground or an excited state, if allowed by the above energy conservation law and transition matrix elements. In the level scheme for our model Helium atom Fig. 6, autoionizing states above the single ionization threshold ($\mathcal{E} > -1.4834$) but below $\mathcal{E} = -0.7722$ have the only possibility to decay towards the ionic bound state that is the ground ionic state. Autoionizing states above $\mathcal{E} = -0.7722$ may decay also to the first excited ionic state plus a less energetic photo-electron.

We first investigate the decay dynamics of such states by solving the TDSE. We then map the solution of the TDSE to construct the exact KS Hamiltonian and the orbital. Furthermore we construct a superposition of the two autoionizing states and compute the decay dynamics within TDDFT. The features observed in the exchange-correlation po-

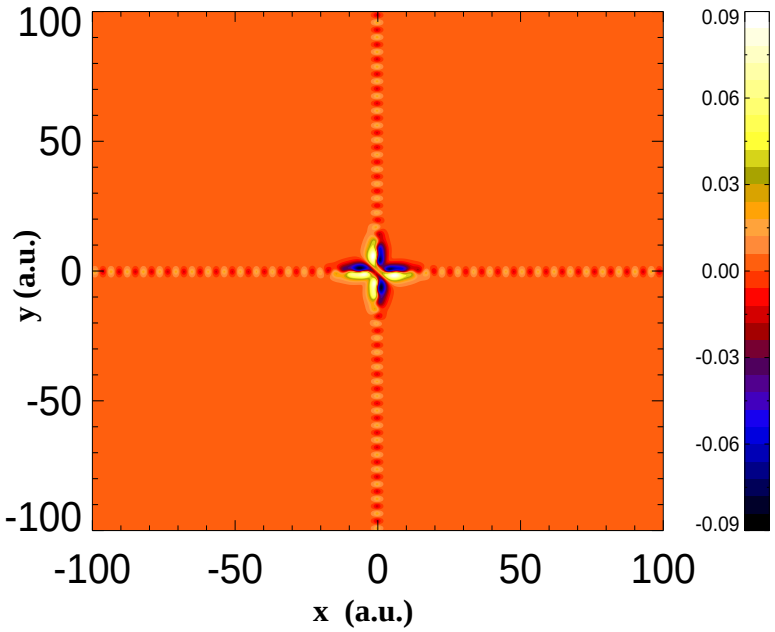

Figure 22: The lowest autoionizing state wave function AI_1 (real-part), corresponding to $\mathcal{E}_{AI_1} = -0.884$. The extended outgoing wave is a feature of such doubly excited states.

tential will shed new light on how such a correlated process may be described within TDDFT.

6.1 dynamical wavepacket evolution from the tdse solution

To study the autoionization dynamics, we select three autoionizing states. The first one is the lowest lying spin-singlet state $\mathcal{E}_{AI_1} = -0.884$ just above the single ionization threshold. The second state is the second lowest lying spin-singlet state $\mathcal{E}_{AI_2} = -0.816$. The third state is a higher lying spin-singlet autoionizing state with $\mathcal{E}_{AI_3} = -0.538$ which may decay to an ion in the ground state plus a "fast" electron or the ion in an excited state plus a "slower" electron. We compute these autoionizing states via the spectral method (see appendix B). The two lowest-lying autoionizing states are shown in Fig. 22 and Fig. 23. One of the degenerate states (which decay towards the first excited ionic bound state) of the higher-lying autoionizing state is shown in Fig. 24.

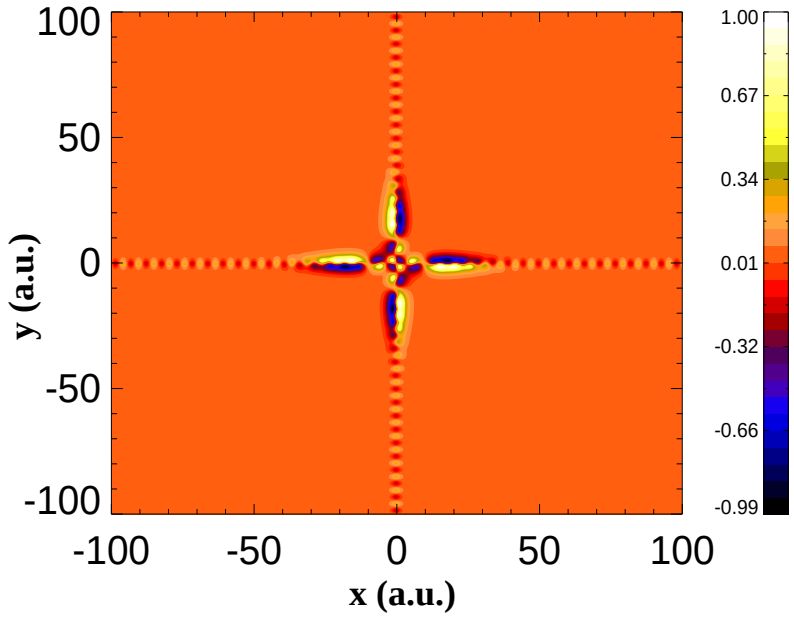

Figure 23: The lowest autoionizing state wave function AI_2 (real-part), corresponding to $\mathcal{E}_{AI_2} = -0.816$.

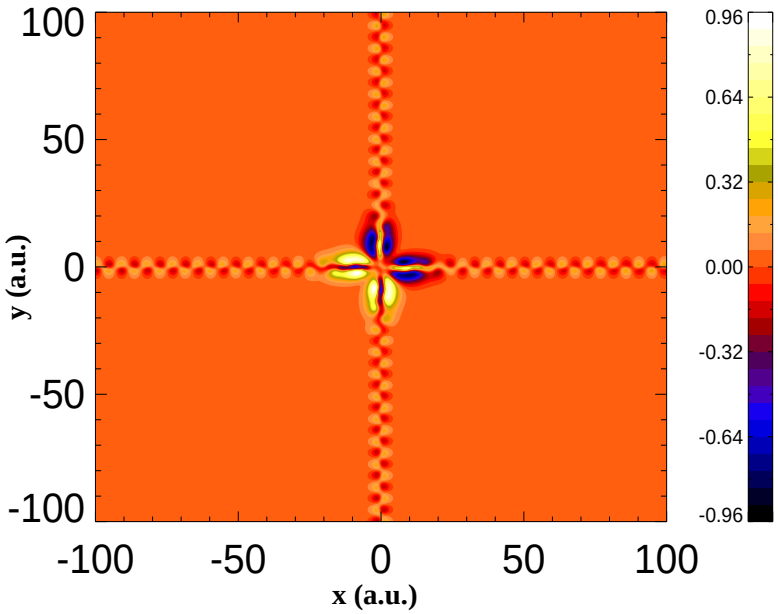

Figure 24: The autoionizing state wave function AI_3 (real-part) above the second ionization threshold, corresponding to $\mathcal{E}_{AI_3} = -0.538$.

To study the decay dynamics we start with the ground state and resonantly couple it to the autoionizing state AI_1. After the laser pulse is switched off the wave function at the end of the laser pulse is propagated further with only the field-free part of the Hamiltonian. In Fig. 25 we plot the wavepackets in a single ionization channel at different time instances and observe that the center of the wavepacket moves with momentum k of the emitted electron. The first wavepacket seen is produced via both the autoionization and the photoionization, while the trailing wavepacket is produced exclusively due to autoionization. The remaining bound electron is seen to be in the nodeless ground ionic state.

After the decay of the highest-lying autoionizing state considered AI_3 the remaining bound electron may be either in the nodeless ground ionic state or the nodal first excited ionic state, as seen in Fig. 26. The center of the wavepackets move with the expected two possible k of the emitted electron. For longer times only the probability density representing the slow photo-electron and the remaining bound electron in the excited state remains.

6.2 mapping the solution to the KS system

Having studied the process by solving the TDSE, we now investigate the TDDFT perspective. With just one spatial orbital it is interesting to see how such a correlated process of autoionization can be reproduced in TDDFT because the orbital, via entering the exchange-correlation potential, has to govern its own decay. Previous studies of the autoionization process within TDDFT have been concentrated on the linear response regime [70]. It is well known that doubly excited states (such as autoionizing ones) will only be described in a TDDFT treatment if the exchange-correlation kernel is frequency-dependent [7]. In this Chapter we will calculate the exact exchange-correlation potential beyond the linear response regime from the solution of the TDSE for autoionization. We start with the autoionizing state AI_1, computed via the spectral method, and determine the exact KS potential and orbital via the technique described in section 3.3.5. In order to account for temporal and spatial loss of the density reaching the boundaries, we modify the exact KS density by including the lost parts of the probability density in the TDSE simulation because of the absorbing boundaries. Otherwise the reconstructed exact exchange-correlation potential would be incorrect. The

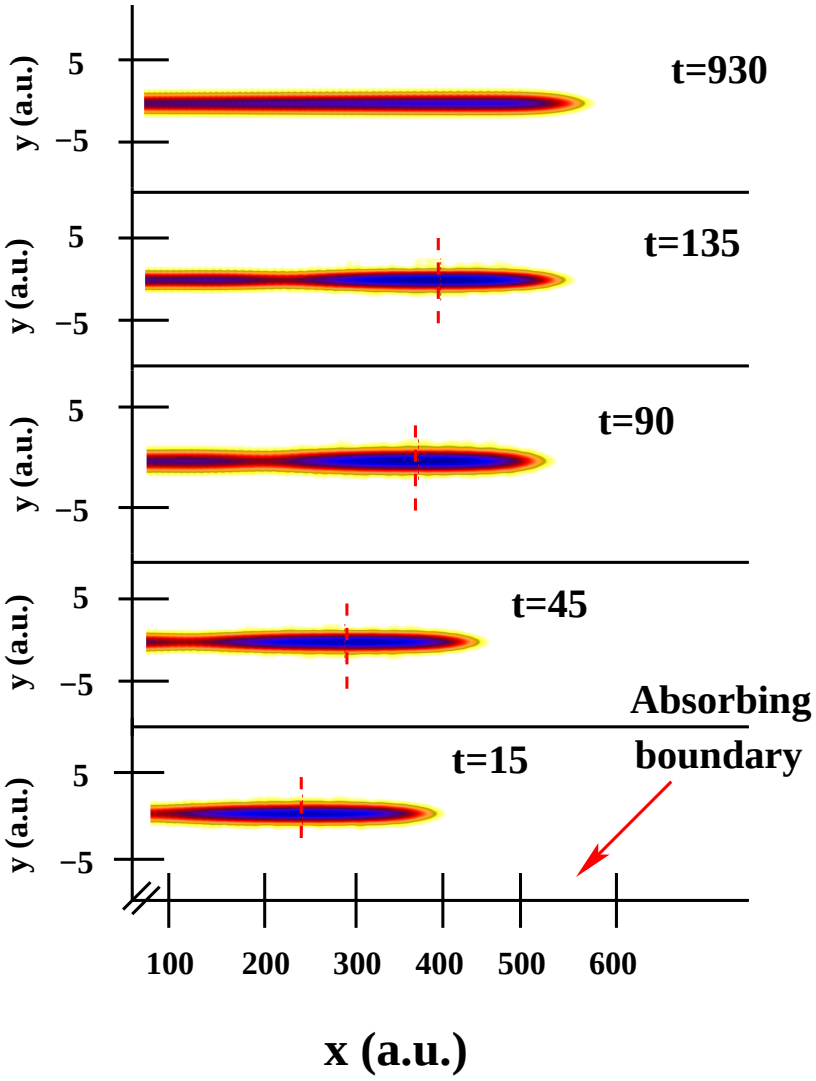

Figure 25: Logarithmic plot of the probability densities in the single ionization channel at different time instants after the laser has been switched off. Vertical red lines indicate the classically expected position of wavepacket with momentum k. Also indicated is the absorbing boundary.

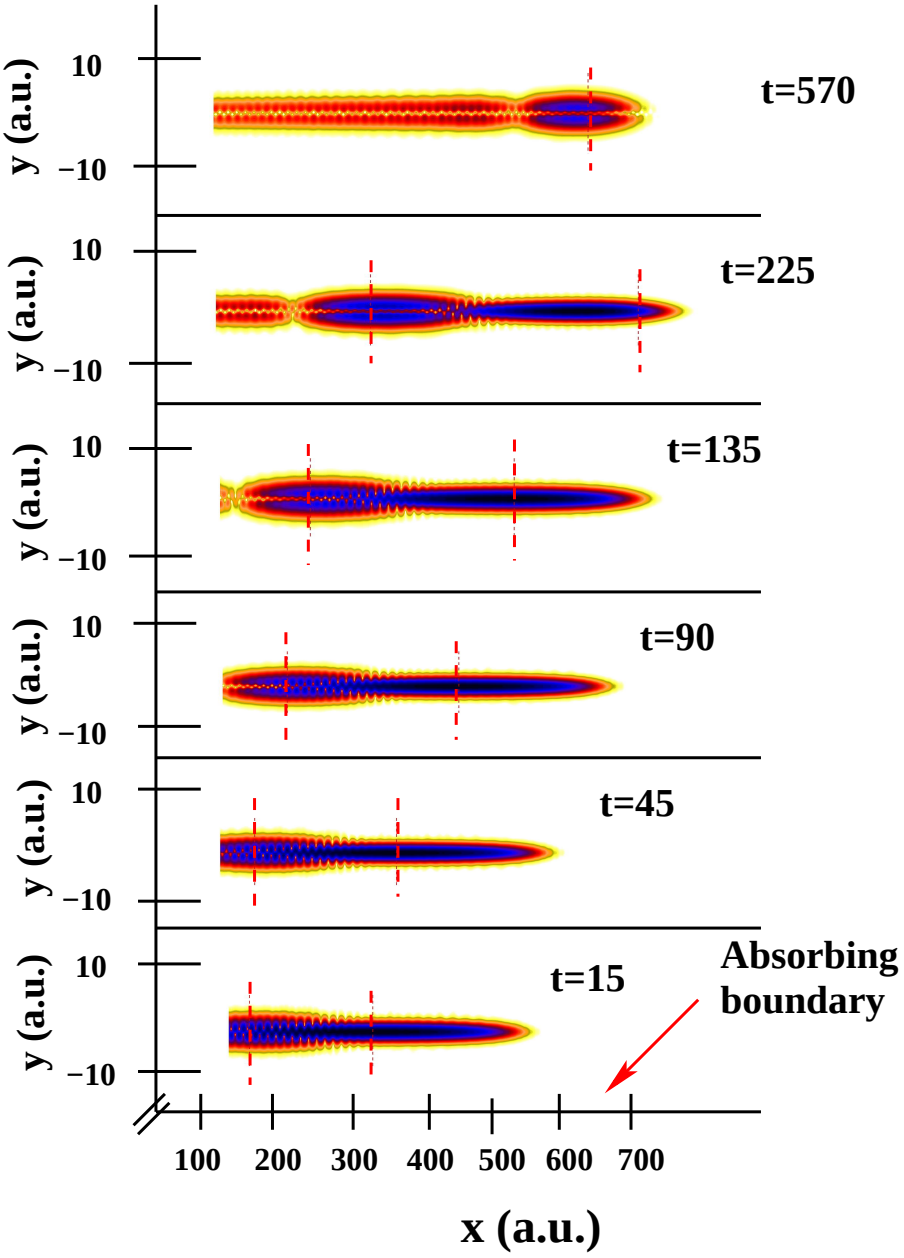

Figure 26: Same as in Fig.25 but for autoionizing state AI_3.

loss terms can be computed from the grid geometry as shown earlier in Fig. 4. The total temporal loss is $(1 - N(t))$, $N(t)$ being the TDSE norm defined in section 3.1.2. The absorbed probability density describes the He^+ ground state as this is the only state found in the single ionization channels in the TDSE simulations as shown in Fig. 25. The exact KS density is then given by

$$n^{\text{corr}}(x,t) = n(x,t) + (1 - N(t))n_{\text{He}^+}. \tag{145}$$

The exact KS potential is then computed with this density. The exact potential and the orbital for the autoionizing state AI_1 at different time instants are shown in Fig. 27. The potential displays features which explain how the density decays. The essential feature is the barrier which the potential develops and through which the corresponding orbital decays via tunneling. Outside the barrier the orbital is a plane-wave with wavevector k, determined via the energy conservation equation (144). Due to our density corrector step we are able to see the orbital asymptotically approaching the He^+ ground state shape. The height and the width of the barrier govern the decay rate while the binding well in the center adjusts for the correct k.

The dynamics of autoionization can also be studied via resonant laser coupling of the ground and the autoionizing state. From the solution of the TDSE we compute the exact KS potential and orbital while the laser pulse is on. In Fig. 28 we see that the initial KS potential is simply the ground state potential of the Helium atom. With population transfer to the autoionizing state, the KS potential starts developing barriers. The height and width of the barrier is dynamically adjusted so that the KS orbital exhibits the correct decay dynamics. This allows the orbital to tunnel out with a proper decay rate.

6.2.1 *Superposition of autoionizing states*

For a superposition of two autoionizing states the KS potential has to control the emission of the photo-electron with two possible different wavevectors. In order to see how this is achieved by just a single spatial KS orbital in its corresponding exchange-correlation potential, we consider the lowest autoionizing state AI_1 and the second lowest autoionizing state AI_2. An equal superposition of the two states is created, and the superposed state is propagated with the field-free part of the Hamil-

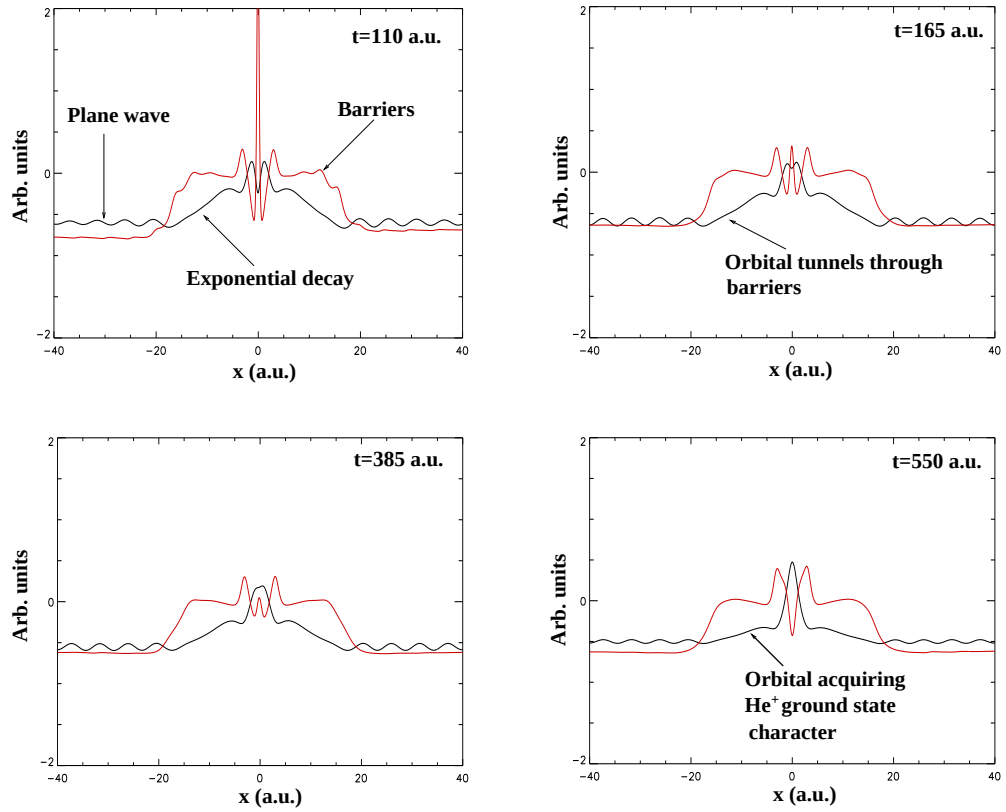

Figure 27: The exact KS potential (red) and the corresponding orbital (black), computed from the initial autoionizing state AI_1. The exact KS potential and orbital are shown at different time instances, as labelled.

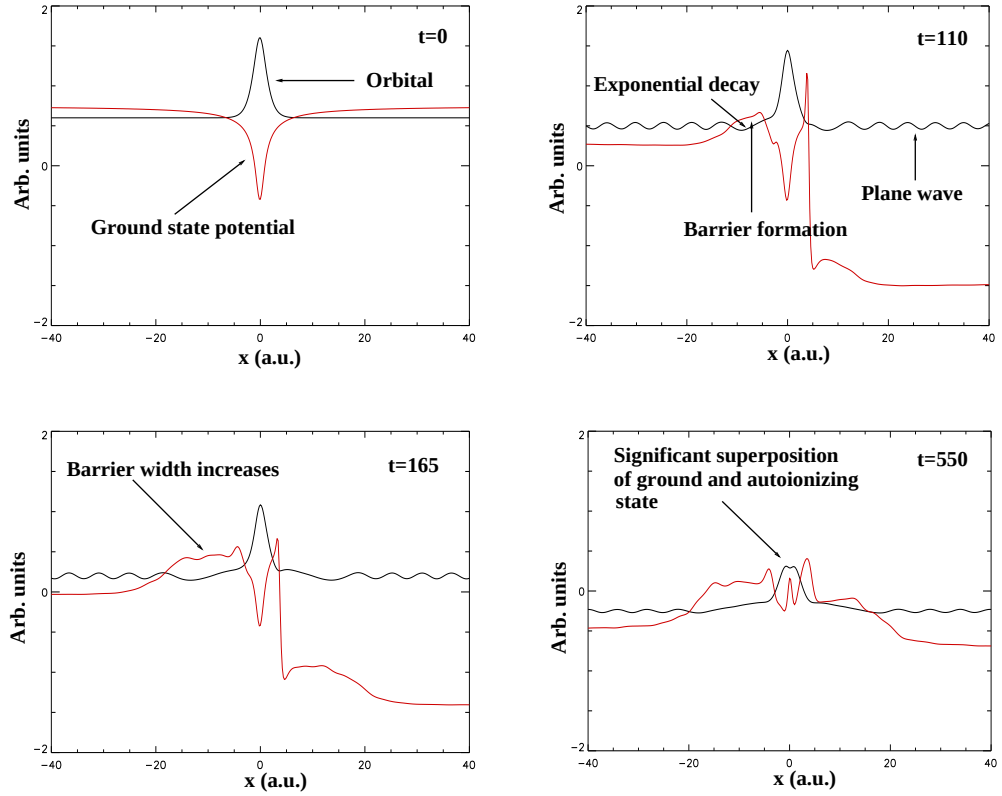

Figure 28: The exact KS potential (red) and the corresponding orbital (black), computed for resonant laser coupling of the ground and the autoionizing state AI_1. The exact KS potential and orbital are shown at different time instances, as labelled.

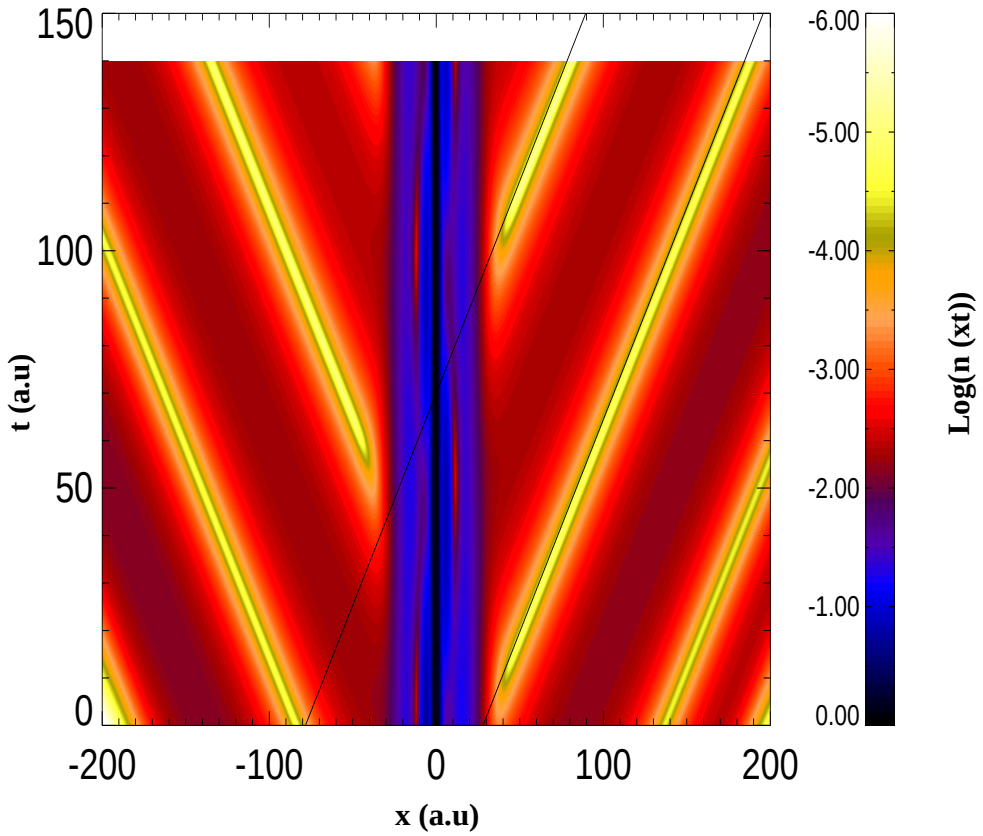

Figure 29: The exact KS orbital density plotted on a log scale. The oblique lines match with the over-plotted lines with the slope $\left|\frac{k_{\mathrm{AI}_2}-k_{\mathrm{AI}_1}}{\mathcal{E}_{\mathrm{AI}_2}-\mathcal{E}_{\mathrm{AI}_1}}\right| = \left|\frac{1.155-1.09}{-0.816+0.884}\right| = 0.88$.

tonian as before [1]. The outgoing density of the orbital oscillates with the momentum difference $k_{\mathrm{AI}_2} - k_{\mathrm{AI}_1}$ in space and oscillates with the energy $\mathcal{E}_{\mathrm{AI}_2} - \mathcal{E}_{\mathrm{AI}_1}$ in time. The density plotted on a log scale as a function of space and time exhibits oblique lines whose slope is the ratio of momentum difference to energy difference. This is shown in Fig. 29. The exact KS potential for such a superposition of autoionizing states is shown in Fig. 30. The potential also oscillates with the respective frequencies.

The above results can be explained if we model the outgoing KS orbital as two decaying plane waves superimposed on each other. This assumption is justified as the second electron is in the same bound state for both

[1] Here the density corrector step is omitted

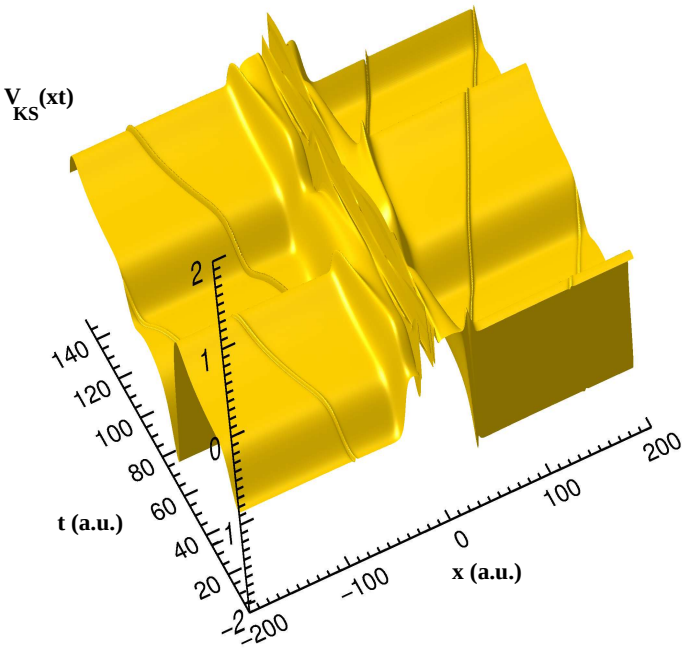

Figure 30: Surface plot of the exact KS potential for an equal superposition of states AI_2 and AI_1. The potential oscillates in time with $\mathcal{E}_{AI_2} - \mathcal{E}_{AI_1}$ and in space with $k_{AI_2} - k_{AI_1}$. Since the oscillation in space is slow, only the oblique lines of Fig. 29 are visible in the space-time plane.

superimposed autoionizing states. The outgoing density $n(x,t)$ in one of the single ionization channels can then be written as

$$\begin{aligned} & n(x,t) \\ = \quad & \left| \exp\left[\mathrm{i}(k_{\mathrm{AI}_1} x + \mathcal{E}_{\mathrm{AI}_1} t) - \frac{\Gamma_{\mathrm{AI}_1}}{2} t \right] + \exp\left[\mathrm{i}(k_{\mathrm{AI}_2} x + \mathcal{E}_{\mathrm{AI}_2} t) - \frac{\Gamma_{\mathrm{AI}_2}}{2} t \right] \right|^2 \\ = \quad & \exp(-\Gamma_{\mathrm{AI}_1} t) + \exp(-\Gamma_{\mathrm{AI}_2} t) + 2\exp\left(-\frac{\Gamma_{\mathrm{AI}_1}}{2} - \frac{\Gamma_{\mathrm{AI}_2}}{2} t \right) \times \\ & \cos[(k_{\mathrm{AI}_2} - k_{\mathrm{AI}_1})x + (\mathcal{E}_{\mathrm{AI}_2} - \mathcal{E}_{\mathrm{AI}_1})t] \end{aligned} \tag{146}$$

Here, $\Gamma_{\mathrm{AI}_1}, \Gamma_{\mathrm{AI}_2}$ are the decay widths of the autoionizing states, AI_1 and AI_2, respectively. From such an expression it is clear that the density plotted on the log scale would have oblique lines with the slope given by $\frac{k_{\mathrm{AI}_2} - k_{\mathrm{AI}_1}}{\mathcal{E}_{\mathrm{AI}_2} - \mathcal{E}_{\mathrm{AI}_1}}$.

Hence, for a superposition of two autoionizing states we obtain an oscillating barrier where the temporal oscillations result from the energy difference of the superposed state and the spatial oscillations result from the momentum difference of the emitted electron. From these results we can see that any approximate exchange-correlation potential would need to accurately reproduce very system-specific features so as to have the correct barrier parameters which ensure the correct decay rate of a particular state. This prohibits in practice the construction of universal approximations to exchange-correlation potentials for the process of autoionization. A more promising route seems to switch to a more differential basic variable instead of the single electron density, for instance time-dependent reduced density matrix theory [71].

7

CONCLUSIONS

Floquet and TDDFT both are promising candidates to simplify the problem of many-body systems in non-perturbative time-periodic drivers such as laser fields. If both could be applied the periodic time-dependent many-body problem could be reduced to a set of time-independent Kohn-Sham-Floquet equations. In this thesis it has been shown that this, unfortunately, is not possible in general.

In Chapter 4, we introduced a method for obtaining information about the field-dressed states (Floquet states) from real-time wave functions. In this approach, it is not necessary to assume strict time-periodicity as in the "standard" Floquet approach. In fact, it is possible to follow the time-resolved Floquet quasi-energies as they shift during a laser pulse. Moreover, the populations of the Floquet states can be determined so that especially cases where superpositions of Floquet states play a role can be identified. The usefulness of the method was illustrated with several examples, employing the one-dimensional Pöschl-Teller potential with only a single field-free bound state. In particular, the origin of even harmonics in an inversion-symmetric potential, avoided crossings of field-dressed states induced by a second laser, the properties of Floquet states under time-periodic transformations, the emergence of invariant, observable photo-electron spectra after the laser pulse, and photo-electron enhancements at channel closings were discussed. The method is straightforwardly extendable to three dimensions (see appendix C). The method is most useful for researchers running codes to solve the time-dependent Schrödinger equation in real time. By saving the wave function at selected spatial positions as a function of time during the interaction with the laser field the analysis in terms of light-induced states can be easily performed *a posteriori*. The method appears to be most adequate at high frequencies where the Floquet blocks are clearly separated.

In Chapter 5 the applicability of the Floquet theorem to time-dependent Kohn-Sham Hamiltonians has been investigated. By employing analyt-

ically and numerically exactly solvable counter examples it was shown that, in general, Floquet theory is not compatible with time-dependent density functional theory (TDDFT). The reason is that, while periodic drivers such as laser fields of course render the interacting many-body Hamiltonian periodic, the corresponding Kohn-Sham Hamiltonian, in general, is aperiodic. How the periodicity properties of the single-particle density translate to the Kohn-Sham potential has been discussed. If in the Floquet analysis of the many-body time-dependent Schrödinger wave function more than one Floquet state plays a role—such as for non-adiabatic ramping or resonant interactions—the exact Kohn-Sham potential is aperiodic so that the Floquet theorem is inapplicable. Further, it has been shown that also the initial-state dependence of the time-dependent Kohn-Sham Hamiltonian cannot be employed to restore its periodicity. Of course, one may view Kohn-Sham-Floquet theory as an approximative approach for the study of laser-matter phenomena in which resonances and non-adiabaticities are expected to be not relevant.

TDDFT employing known and practicable exchange-correlation potentials does not capture highly correlated electron dynamics or resonant interactions. Autoionization in a two-electron system such as the Helium atom is one of the most correlated processes and thus serves as an interesting testing ground for any method going beyond "standard" TDDFT. In Chapter 6 the exact Kohn-Sham potential and orbital has been constructed for an autoionizing model Helium atom. It was shown that the exact Kohn-Sham potential develops barriers through which the Kohn-Sham orbital decays. The decay rate is governed by the barrier parameters in a very intricate way such that the correct lifetime of the autoionizing state is recovered. Approximate exchange-correlation potentials capturing such dynamics would necessarily require memory effects and are unlikely to be developed. Instead, theoretical approaches relying on more differential entities than just the single particle density are more promising avenues towards a proper description of correlated processes in driven many-body systems.

Appendices

A

IMAGINARY TIME PROPAGATION

The initial state is typically either the ground state or an excited state of the system. To obtain the ground state $n = 0$, consider the stationary Schrödinger equation

$$\hat{H}_0|\Psi_n\rangle = \mathcal{E}_n|\Psi_n\rangle. \tag{147}$$

Then starting from an initial guess for the wave function which can be expanded in terms of the eigenfunctions $|\Psi_n\rangle$,

$$|\Psi\rangle = \sum_n c_n|\Psi_n\rangle, \tag{148}$$

the wavefunction propagated one imaginary timestep reads

$$|\Psi(-\mathrm{i}\delta t)\rangle = \sum_n c_n \exp(-\mathcal{E}_n\delta t)|\Psi_n\rangle. \tag{149}$$

For successive propagation in imaginary time the ground state $|\Psi_0\rangle$ decays most slowly. Hence asymptotically only the ground state "survives". As imaginary time-propagation is not unitary the wave function has to be renormalized.

In order to obtain the excited states of the system, the Gram-Schmidt orthogonalization procedure is applied. In this procedure, we first obtain the ground state and start with an initial guess for the first excited state. The imaginary time propagation is performed as above where at each imaginary timestep the previously obtained ground state is out-projected,

$$|\Psi_1\rangle - \langle\Psi_0|\Psi_1\rangle|\Psi_0\rangle, \tag{150}$$

and the result normalized. In that way asymptotically the first excited state is obtained.

Normalizing $|\Psi_1\rangle$ at each timestep gives the first excited state of the system after a sufficient number of timesteps. This method is practicable if only a few low-lying excited states are required. For high-lying excited

states and quasi-bound states the spectral method of Feit, Fleck and Steiger [33] is more suitable and will be subsequently explained.

B

SPECTRAL METHOD FOR THE TIME DEPENDENT SCHRÖDINGER EQUATION

A straightforward way of obtaining high-lying excited or quasi-bound states is provided by the spectral method [33] where we start from a guess wave function and propagate it in real-time with the field-free Hamiltonian (18), leading to

$$|\Psi(t)\rangle = \sum_n \exp(-\mathrm{i}\mathcal{E}_n t)|\Psi_n\rangle. \tag{151}$$

While propagating $|\Psi(t)\rangle$ it is multiplied by $\exp(\mathrm{i}\mathcal{E}t)$ where $\mathcal{E}$ is the target energy of the desired state. Integrating over a sufficiently long time interval,

$$|\Psi_\mathcal{E}\rangle \sim \int_0^T \exp(\mathrm{i}\mathcal{E}t)|\Psi(t)\rangle \mathrm{d}t, \tag{152}$$

only the state for which the phase is stationary, i.e., $\mathcal{E} = \mathcal{E}_n$ "survive" and the eigenstate $|\Psi_\mathcal{E}\rangle$ is obtained.

The quasi-bound states obtained via this method for the Helium model system were shown in Fig. 22, Fig. 23 and Fig. 24 for $T \approx 5000$. The state whose energy lies closest to the target energy will be obtained.

Appendix B: spectral method for the time dependent schrödinger equation

C

FLOQUET ANALYSIS IN THREE DIMENSIONS

The method of Floquet analysis described in Chapter 4 is easily extendable to higher-dimensional systems. For, e.g., hydrogenic systems in three dimensions one could follow the evolution of Floquet states with different orbital angular momentum quantum numbers l. Instead of (39) let us write

$$\Psi(r,\theta,\phi,t) = e^{-i\epsilon t}\Phi(r,\theta,\phi,t) \tag{153}$$

with [compare to (44)]

$$\Phi(r,\theta,\phi,t) = \sum_n \varphi_n(r,\theta,\phi)\mathrm{e}^{-in\omega_1 t}. \tag{154}$$

The operator $\hat{P}_{pt}$ [compare to (51)] acts according

$$\hat{P}_{pt}f(\boldsymbol{r},t) = f(-\boldsymbol{r},t+\frac{\pi}{\omega}) \tag{155}$$

and (54) becomes

$$\hat{P}_{pt}\Phi(r,\theta,\phi,t) = \sum_n (-1)^n \exp(-in\omega_1 t)\hat{P}_p\varphi_n(r,\theta,\phi). \tag{156}$$

If we expand the $\varphi_n(r,\theta,\phi)$ in spherical harmonics,

$$\varphi_n(r,\theta,\phi) = R_{nl}(r)Y_{lm}(\theta,\phi), \tag{157}$$

we find, using

$$\hat{P}_p Y_{lm}(\theta,\phi) = Y_{lm}(\pi-\theta,\pi+\phi) = (-1)^l Y_{lm}(\theta,\phi), \tag{158}$$

that

$$\hat{P}_p\varphi_n(r,\theta,\phi) = (-1)^{n+l}\varphi_n(r,\theta,\phi), \tag{159}$$

the analogue of (55). Note that n is the Floquet block index here, not the principal quantum number. After these considerations it is straightforward to extend the Floquet analysis of real-time wavefunctions described in this work to 3D.

BIBLIOGRAPHY

[1] M.G. Floquet, Ann. Écol. Norm. Sup. **12**, 47 (1883).

[2] J.H. Shirley, Phys. Rev. **138**, B979 (1965); H. Sambe, Phys. Rev. A **7**, 2203 (1973).

[3] Floquet theory is covered in several text books, e.g., D.J. Tannor, *Introduction to Quantum Mechanics: a Time-Dependent Perspective* (University Science Books, Sausalito, 2007); B.H. Bransden, C.J. Joachain, *Physics of Atoms and Molecules* (Prentica Hall, Harlow, 2003); H. Friedrich, *Theoretical Atomic Physics*, (Springer, Berlin, 2006); F.H.M. Faisal, *Theory of Multiphoton Processes* (Plenum Press, New York, 1987).

[4] S.-I. Chu, D.A. Telnov, Phys. Rep. **390**, 1 (2004).

[5] P. Hohenberg, W. Kohn, Phys. Rev. **136**, B864 (1964).

[6] See, e.g., R. M. Dreizler and E. K. U. Gross, *Density Functional Theory, An Approach to the Quantum Many-Body Problem* (Springer, Berlin, 1990).

[7] See, e.g., C. A. Ullrich, *Time-Dependent Density-Functional Theory* (Oxford University Press, New York, 2012); M. A. L. Marques et al., *Time-Dependent Density Functional Theory* (Springer, Heidelberg, 2006).

[8] W. Kohn, Rev. Mod. Phys. **71**, 1253 (1999).

[9] W. Kohn and L. J. Sham. Phys. Rev. **140**, A1133 (1965).

[10] E. Runge and E. K. U. Gross, Phys. Rev. Lett. **52**, 997 (1984).

[11] R. van Leeuwen, Phys. Rev. Lett. **82**, 3863 (1999).

[12] M. Ruggenthaler and D. Bauer, Phys. Rev. A **80**, 052502 (2009).

[13] F. Wilken and D. Bauer, Phys. Rev. Lett. **97**, 203001 (2006); F. Wilken and D. Bauer, Phys. Rev. A **76**, 023409 (2007).

[14] M. Ruggenthaler and D. Bauer, Phys. Rev. Lett. **102**, 233001 (2009).

[15] J. I. Fuks, N. Helbig, I. V. Tokatly, and A. Rubio, Phys. Rev. B **84**, 075107 (2011).

[16] P. Agostini, F. Fabre, G. Mainfray, G. Petite, and N. Rahman, Phys. Rev. Lett. **42**, 1127 (1979).

[17] D. B. Milošević, G. G. Paulus, D. Bauer, and W. Becker, J. Phys. B **39**, R203 (2006).

[18] G. G. Paulus, W. Nicklich, F. Zacher, P. Lambropoulos and H. Walther, J. Phys. B: At. Mol. Opt. Phys. **29** (1996).

[19] J. L. Krause, K. J. Schafer, and K. C. Kulander, Phys. Rev. Lett. **68**, 3535 (1992).

[20] See, e.g., P. Mulser and D. Bauer *High Power Laser-Matter Interaction* (Springer, Berlin, Heidelberg, 2010).

[21] B.H. Bransden, C.J. Joachain, *Physics of Atoms and Molecules* (Prentica Hall, Harlow, 2003).

[22] J. J. Sakurai, *Advanced quantum mechanics* (1967).

[23] Ruiz C, Plaja L and Roso L Phys. Rev. Lett. **94** 063002 (2005).

[24] R. Grobe and J. H. Eberly, Phys. Rev. A **48**, 4664 (1993).

[25] D. Bauer, Phys. Rev. A **56**, 3028 (1997).

[26] S. L. Haan, R. Grobe, and J. H. Eberly, Phys. Rev. A **50**, 378 (1994).

[27] M. Lein, E. K. U. Gross, and V. Engel, Phys. Rev. A **64**, 023406 (2001).

[28] R. Grobe and J. H. Eberly, Phys. Rev. Lett. **68**, 2905 (1992).

[29] D. Bauer, Phys. Rev. A **56**, 3028 (1997).

[30] D. G. Lappas and R. van Leeuwen, J. Phys. B **31**, L249 (1998).

[31] M. Lein, E. K. U. Gross, and V. Engel, Phys. Rev. Lett. **85**, 4707 (2000).

[32] F. Wilken, *Density Functional Treatment of Atomic Strong-Field Ionization Processes* (University of Heidelberg, 2006).

[33] M.D. Feit, J.A. Fleck, A. Steiger, J. Comput. Phys. **47**, 412 (1982).

[34] J. Zhao and M. Lein, New J. Phys. **14**, 065003 (2012).

[35] M. O. Scully and M. Suhail Zubairy, Quantum Optics (Cambridge University Press, Cambridge, England, 2001).

[36] O. E. Alon, V. Averbukh, N. Moiseyev, Phys. Rev. Lett. **80**, 3743 (1998); O.E. Alon, Phys. Rev. A **66**, 013414 (2002).

[37] F. Ceccherini, D. Bauer, F. Cornolti, J. Phys. B: At. Mol. Opt. Phys. **34**, 5017 (2001).

[38] T. Kato, Commun. Pure Appl. Math., **10**, 151-77 (1957).

[39] M. Lein and S. Kümmel, Phys. Rev. Lett. **94**, 143003 (2005).

[40] I. D Amico and G. Vignale, Phys. Rev. B **59**, 7876 (1999).

[41] M. Ruggenthaler, S.E.B. Nielsen, R. van Leeuwen, Phys. Rev. A **88**, 022512 (2013).

[42] J. D. Ramsden and R. W. Godby, Phys. Rev. Lett. **109**, 036402 (2012).

[43] S.E.B. Nielsen, M. Ruggenthaler, R. van Leeuwen, Europhys. Lett **101**, 33001 (2013).

[44] V. Kapoor, M. Ruggenthaler, D. Bauer, Phys. Rev. A **87**, 042521 (2013)

[45] J. I. Fuks, P. Elliott, A. Rubio, and N. T. Maitra, J. Phys. Chem. Lett. **4**, 735 (2013).

[46] D.A. Telnov, S.- I. Chu. Chem. Phys. Lett. **264**, 466 (1997).

[47] M. Gavrila, J. Phys. B: At. Mol. Opt. Phys. **35**, R147 (2002).

[48] V. Kapoor, D. Bauer, Phys. Rev. A **85**, 023407 (2012).

[49] M. Richter, S. Patchkovskii, F. Morales, O. Smirnova and M. Ivanov, New J. Phys. **15**, 083012 (2013).

[50] R. Bavli, H. Metiu, Phys. Rev. A **47**, 3299 (1993).

[51] N. Moiseyev, M. Lein, J. Phys. Chem. A **107**, 7181 (2003).

[52] A. Di Piazza, E. Fiordilino, Phys. Rev. A **64**, 013802 (2001).

[53] T. Timberlake, L.E. Reichl, Phys. Rev. A **59**, 2886 (1999).

[54] S.S. Shamailov, A.S. Parkins, M.J. Collett, H.J. Carmichael, Opt. Comm. **283**, 766 (2010).

[55] W. Becker, F. Grasbon, R. Kopold, D.B. Milošević, G.G. Paulus, H. Walther, Adv. At. Mol. Opt. Phys. **48**, **35** (2002).

[56] See, e.g., P. Mulser, D. Bauer, *High Power Laser-Matter Interaction* (Springer, Berlin Heidelberg, 2010), Chap. 7.

[57] D.B. Milošević, G.G. Paulus, D. Bauer, W. Becker, J. Phys. B: At. Mol. Opt. Phys. **39**, R203 (2006).

[58] B. Fetić, D.B. Milošević, W. Becker, J. Mod. Opt. **58**, 1149 (2011).

[59] J. Wassaf, V. Véniard, R. Taïeb, A. Maquet, Phys. Rev. Lett. **90**, 013003 (2003); Phys. Rev. A **67**, 053405 (2003).

[60] M.P. Hertlein, P.H. Bucksbaum, H.G. Muller, J. Phys. B: At. Mol. Opt. Phys. **30**, L197 (1997); P. Hansch, M.A. Walker, and L.D. van Woerkom, Phys. Rev. A **55**, R2535 (1997).

[61] S.V. Popruzhenko, Ph.A. Korneev, S.P. Goreslavski, W. Becker, Phys. Rev. Lett. **89**, 023001 (2002).

[62] Neepa T. Maitra, Kieron Burke, Chris Woodward, Phys. Rev. Lett. **89**, 023002 (2002); Neepa T. Maitra and Kieron Burke, Phys. Rev. A **63**, 042501 (2001); Phys. Rev. A **64**, 039901(E) (2001).

[63] B. M Deb, S. K. Ghosh, J. Chem. Phys. **77**, 342 (1982).

[64] D. W. Hone, R. Ketzmerick, and W. Kohn, Phys. Rev. A **56**, 4045 (1997).

[65] Pawel Salek, Trygve Helgaker, Trond Saue, Chem. Phys. Lett. **311**,187 (2005).

[66] D.A. Telnov, S.-I. Chu. Phys. Rev. **58**, 6 (1998).

[67] N. T. Maitra, K. Burke, Chem. Phys. Lett. **359**, 237 (2002).

[68] N.T. Maitra, K. Burke, Chem. Phys. Lett. **441**, 167 (2007).

[69] U. Fano, Physical Review, **124**, 6 (1961).

[70] AJ. Krueger and Neepa T. Maitra, Phys. Chem. Chem. Phys. **11**, 4655-4663 (2009).

[71] M. Brics, D. Bauer, Phys. Rev. A **88**, 052514 (2013).

ERKLÄRUNG

Ich versichere hiermit an Eides statt, dass ich die vorliegende Arbeit selbstständig angefertigt und ohne fremde Hilfe verfasst habe. Dazu habe ich keine außer den von mir angegebenen Hilfsmitteln und Quellen verwendet, und die den benutzten Werken inhaltlich und wörtlich entnommenen Stellen habe ich als solche kenntlich gemacht.

Rostock, January 8, 2014

Varun Kapoor